Title
Conjugating CRISPR-Cas9 Machinery to Single-Walled Carbon Nanotubes for Plant Cellular Delivery

Author
Cunningham, Francis

Publication Date
2021

Peer reviewed|Thesis/dissertation

Conjugating CRISPR-Cas9 Machinery to Single-Walled Carbon Nanotubes for Plant Cellular Delivery

by

Francis J Cunningham

A dissertation submitted in partial satisfaction of the

requirements for the degree of

Doctor of Philosophy

in

Chemical Engineering

in the

Graduate Division

of the

University of California, Berkeley

Committee in charge:

Professor Markita Landry, Chair

Professor Wenjun Zhang

Professor James Cate

Summer 2022

Abstract

Conjugating CRISPR-Cas9 Machinery to Single-Walled Carbon Nanotubes for Plant Cellular Delivery

by

Francis J Cunningham

Doctor of Philosophy in Chemical Engineering

University of California, Berkeley

Professor Markita Landry, Chair

Introducing CRISPR machinery to a host plant genome may be accomplished either through expression of recombinant plasmids or direct delivery of the Cas9 ribonucleoprotein (RNP). However, introducing the biomolecular workhorses of CRISPR into model and crop species is hindered by the molecular delivery challenge across the plant cell wall. The cell wall presents a rigid barrier to biomolecule delivery which can be overcome by Agrobacterium or biolistic particle bombardment, the success of which is limited by host species, tissue type, and random transgene integration. Furthermore, the necessity of tissue culture introduces further limitations, as many crops are recalcitrant towards regeneration. RNP delivery simplifies the workflow of plant gene editing by circumventing the need for plasmid optimization and improves specificity by reduction of off-target cleavage. However, introducing Cas9 RNPs into plants is not easily addressed by current delivery technologies, as *Agrobacterium* is only amenable to DNA delivery and biolistics rely on protein dehydration which can result in loss of Cas9 activity.

Nanomaterials offer an addition to the workhorses of plant genetic engineering due to their ability to load diverse cargo, traverse the cell wall and plasma membrane, and selectively localize in tissues and organelles. We have developed a polyamine-carbon nanotube conjugate (PEI-SWNT) which is loaded with DNA and administered by aqueous infiltration to the leaf abaxis. In *Nicotiana benthamiana*, we report indel generation in a GFP transgene via PEI-SWNT plasmid delivery. We also present the development of Cas9-SWNT conjugates for RNP delivery to mature plant tissue without biolistics – both through direct binding of an engineered Cas9 variant to the CNT surface and through the inclusion of a noncovalent peptoid intermediate for binding of WT Cas9 to the CNT surface. Peptoids, or poly-*N*-substituted glycines, possess remarkable biostability and peptide-like structural properties. We present the design and synthesis of modular peptoids with two domains, a CNT-binding domain and an RNP-binding domain, and demonstrate screening of a peptoid library based on these domains for non-covalent binding of Cas9 to peptoid-CNTs. We have identified charge and the protein:SWNT ratio as key variables in the design of a stable conjugate, where a stable RNP-peptoid-conjugate can then enable cytosolic delivery of preassembled Cas9 RNP to mature plant cells. Lastly, we report indel generation in the model gene target *phytoene desaturase* (PDS) from *N. benthamiana* via peptoid-SWNT mediated delivery of Cas9 RNPs.

Table of Contents

1. Traditional Plant Breeding and the Green Revolution

For many thousands of years plants have undergone artificial selection by humans, leading to the emergence of crop cultivars with massively enhanced productivity traits compared to their wild relatives. Traditional plant breeding—a process of hybridization between two elite parent lines and repeated backcrossing of the progeny with one of its parents—relies on classical Mendelian genetics and has long proceeded without any knowledge of a trait's molecular basis. In the mid-20th century, global research initiatives for plant science greatly accelerated this process of artificial selection, ushering in a new era of agriculture known as the Green Revolution. The high-yield crop products of this revolution, in particular semidwarf rice and wheat were a critical sustaining element of the global population boom in the last half-century.[1] Semidwarf crop varieties exhibit shorter stalk heights at adulthood, thus shrinking the time to harvest and, in the case of cereal crops such as rice, allowing the plant to direct biomass production towards grains. For example, since the introduction of semidwarf high-yield rice varieties (IR rice) developed by the International Rice Research Institute in the 1960s-70s, global rice production has increased from approximately 200 MM tons in 1961 to 1500 MM tons in 2002, while the average price for rice has fallen from $300/ton to $75/ton along the same time period.[2] Notably, despite this enormous boost in production, the global footprint for rice farms has barely increased, from 300 MM acre in 1961 to 345 MM acre in 2000, compared to the 740 MM acre that would have been required to meet demand at 1961 yield levels.[2] However, increased yield is not the only important trait – biotic and abiotic stress resistance is also critical for a crop to maintain success across harvests and within different agricultural environments. The original high-yield IR rice variety had virtually no resistance to any of the common rice pests; it took over a decade and dozens of crosses to transfer traits from resistant cultivars into the semidwarf variety using traditional breeding methods,[2] in part due to a lack of tools available to understand, manipulate, and transfer resistance genes across cultivars and species.

2. Genome Editing in Plant Breeding

Despite the immense impact that plant breeding programs have had on the global agricultural industry, as evidenced through the success of semidwarf IR rice, there still exists major drawbacks to this tried and true approach. Through traditional crossing and hybridization methods, it may take up to 10-15 generations to realize a stable cultivar and loss of function products are common. Thus, traditional breeding is generally labor and time-intensive, albeit very effective, in part due to the intrinsically large number of genetic elements that are affected by crossing and hybridization. Several studies agree that current trends in crop production are far too slow to meet the projected 100% increase in global demand by 2050.[4] Thus, there exists a need for rapid innovation in the plant breeding sector – a need that can be met by genetic engineering. Modern biotechnology has expanded plant breeding into the realm of targeted genetic modification through the rise of genome editing technologies such as those derived from Clustered Regularly Spaced Short Palindromic

Repeat (CRISPR) systems. Recently, CRISPR was applied in *Musa acuminate* (banana) for a gene knockout resulting in a semidwarf phenotype similar to the one found in IR rice[5] – a result of particular importance to the utility of CRISPR in breeding, as cultivated banana is parthenocarpic (sterile) and therefore not easily bred by traditional means. The semidwarf phenotype has also been achieved using CRISPR in *Brassica napus L.* (canola).[6] To date, CRISPR has been utilized for yield improvement in *Oryza sativa* (rice) across at least ten gene targets[7], and has been expanded towards many other species including *Glycine max* (soybean)[8,9], *Triticum aestivum* (bread wheat)[10–12], and *Zea mays* (maize).[13]

CRISPR has also demonstrated efficacy for *de novo* domestication in *Solanum lycopersicum* (tomato), in which multiple gene loci of wild tomato were engineered to introduce the enhanced productivity traits of cultivated tomato, such as compact plant architecture, synchronized fruit ripening, day-length insensitivity, enlarged fruit size, and increased vitamin C.[14,15] *De novo* domestication by targeted gene modification is much faster than traditional breeding and avoids the fitness costs associated with Mendelian inheritance, allowing for the retention of abiotic and biotic resistances present in wild cultivars. Notably, CRISPR has been used to domesticate so-called orphan crops – cultivated species whose productivity traits remain severely underdeveloped – such as *Physalis pruinosa* (ground cherry).[16]

In addition to enhancement of productivity traits by yield improvement and *de novo* domestication, CRISPR has been used to introduce novel traits to plants in the form of disease resistance. Much like the natural function of CRISPR in bacteria to fight off phage infection, CRISPR machinery targeting plant viruses can be integrated into the plant genome, as was done in *Solanum tuberosum* (potato) to introduce resistance to multiple strains of *Potato Virus Y*.[17] An alternative strategy to achieving plant viral resistance is to alter endogenous genes known to play a role in viral infection pathways; wherein this method would not require the integration of CRISPR machinery in the final product. This strategy was adopted in *Manihot esculenta* (cassava), in which targeted mutation of a host translation initiation factor known to interact with virulence proteins from *Cassava brown streak virus* resulted in dramatically reduced disease symptoms.[18] Other examples of CRISPR-mediated disease resistance include the fungal pathogen powdery mildew in *T. aestivum* (bread wheat),[19] the bacterial pathogen *Xanthomonas oryzae* in *O. sativa* (rice)[20], and the parasitic weed *Phelipanche aegypytiaca* in *S. lycopersicum* (tomato).[21]

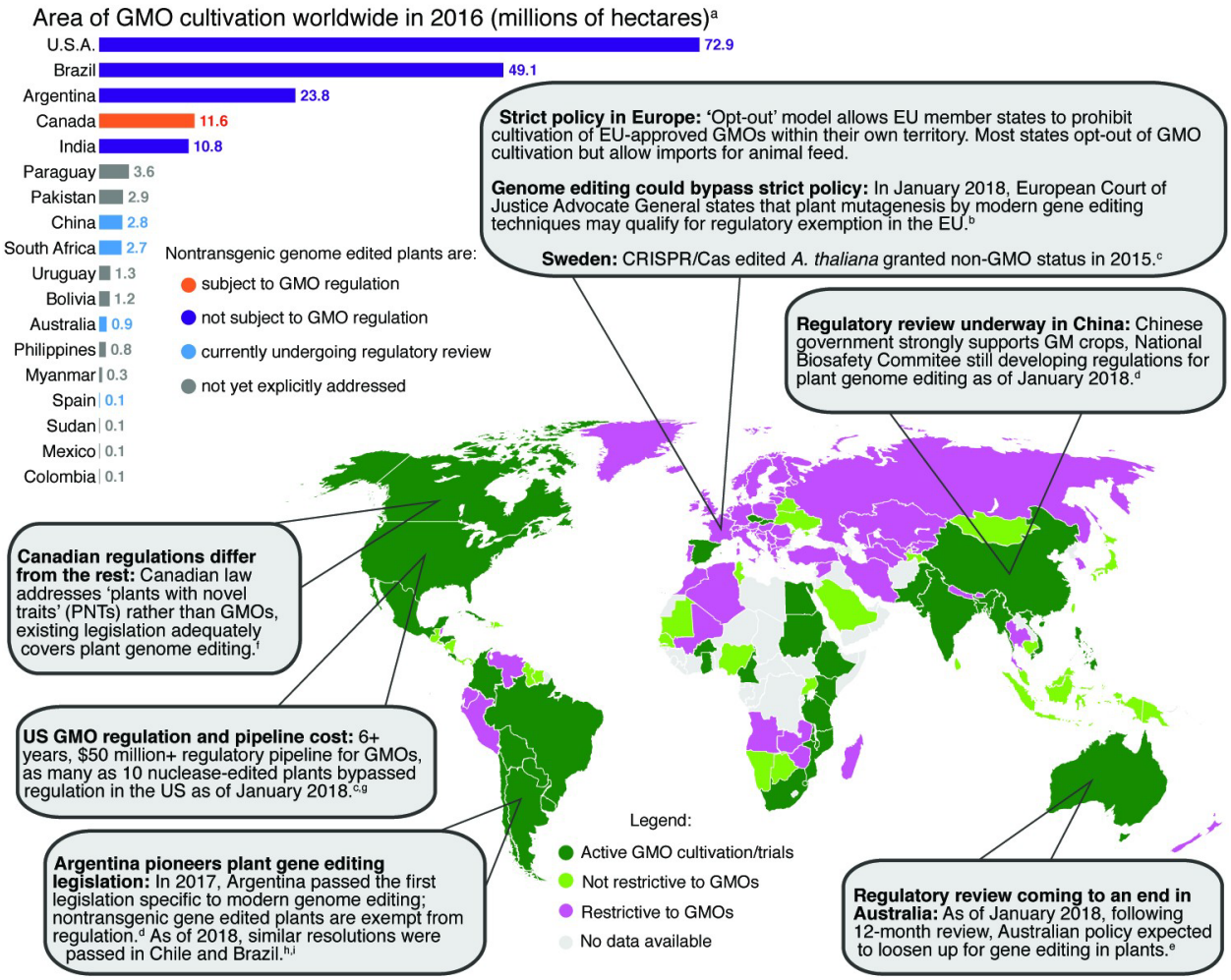

Figure 1: GMO cultivation and regulatory attitudes worldwide. Despite a long, expensive regulatory pipeline, the U.S. is a leader for GMO cultivation worldwide, followed by Brazil and Argentina, with Argentina being the first to directly address modern genome editing techniques in GMO legislation. European and Australian regulatory attitudes are strict but have recently evolved as of January 2018, suggesting that regulations for genome edited plants will soon be relaxed in these regions. Nuclease-based edits without transgene integration escape regulation even in countries with large agricultural GMO industries and complex regulatory systems. Adapted with permission.[3]

3. An Introduction to CRISPR-Cas9

CRISPR was first identified in the 1990s and early 2000s as a family of genes in prokaryotes implicated in adaptive immunity towards bacteriophages through a variety of

targeting mechanisms that degrade invading nucleic acids.[22] In 2012, CRISPR-associated protein 9 (Cas9) from *Streptococcus pyogenes* (spCas9), an RNA-guided DNA endonuclease, was first adapted as an easily programmable tool for genome editing through the development of a synthetic guide RNA (sgRNA) targeting mechanism that directs Cas9 to cleave dsDNA at a specified location.[23] The sgRNA contains two domains: a constant 5' scaffold region (~100 nt) with several stem-loop structures responsible for association with the Cas9 protein, and a variable 3' spacer region (~20 nt) with homology to the target sequence in dsDNA.

The mechanism for Cas9-mediated dsDNA cleavage is as follows.[24] Cas9 directly associates with sgRNA through an arginine-rich binding pocket to form a ribonucleoprotein (RNP) that is now activated for target recognition and cleavage. Through a protein-DNA interaction, Cas9 RNP binds to the protospacer adjacent motif (PAM), a region of DNA directly downstream of the target site specified by the sgRNA, and begins to locally unwind the DNA double helix. PAM binding is a critical initial step in target recognition and so the presence of a PAM in the target sequence is absolutely required for cleavage regardless of sgRNA identity. The canonical PAM for the most well-studied Cas variant, spCas9, is 5'-NGG-3' (where 'N' is any nucleobase) - however, given the abundance of NGG sequences in all genomes, and the discovery of other Cas variants with diverse PAM sequences, the PAM is not practically limiting for targeting a given locus. Once PAM binding and local helix unwinding are initiated, the sgRNA will invade and interrogate the DNA strand opposite of the PAM sequence (i.e. the 'target' strand). If homology exists between the sgRNA and target strand, the sgRNA will fully anneal as the DNA double helix is continually unwound, forming an R-loop structure that is stabilized by the protein. R-loop formation induces enzymatic activity in Cas9, in which the HNH and RuvC domains catalyze cleavage of the phosphodiester bonds on the target and non-target strands, respectively, three base pairs upstream from the PAM.

The result of Cas9 cleavage is a double-stranded break (DSB) at a specified location in target DNA. Once cleavage occurs *in vivo*, endogenous DSB repair mechanisms take over to repair the cut, wherein the primary repair pathways are non-homologous end-joining (NHEJ) and homology-directed repair (HDR). Both of these pathways are known to have critical endogenous functions related to recombination and mitosis, as well as in cells whose genomes have been damaged, e.g. by radiation. NHEJ is the predominant DSB repair pathway in growing G_1 phase cells and proceeds without the need for a homologous repair template by directly ligating the broken ends. While NHEJ typically repairs the DSB accurately, repeated cleavage of the target site may eventually lead to inaccurate repair through the introduction of a small insertion or deletion (indel) mutation. Thus, overexpression of CRISPR machinery in a host cell drives NHEJ repair towards indel formation which can then lead to disrupted function of the target locus (e.g. gene knockout or targeted mutagenesis). In contrast, the HDR pathway occurs predominantly in S and G_2 phase cells and proceeds in the presence of a homologous repair template which is inserted at the site of the DSB. Thus, if a donor repair template co-expressed with the CRISPR machinery is present in a host cell capable of HDR-based repair, then HDR-associated proteins will use the donor template to repair the DSB, resulting in directed insertion of a DNA sequence (i.e. gene knock-in or site-directed mutagenesis). This strategy of hijacking endogenous DSB pathways for nuclease-

based gene editing is not unique to CRISPR systems, as evidenced by the rise of zinc finger nuclease (ZFN), Transcription activator-like effector nuclease (TALEN), and meganuclease based tools in the early 2000s.[25] However, the superior efficiency and simplicity of the RNA-guided targeting mechanism of Cas9 has allowed CRISPR to greatly surpass previous genome editing technologies in recent years. Despite the demonstrated potential of CRISPR for a wide variety of applications in plants, further progress is hindered by substantial limitations in the delivery of CRISPR machinery into plant cells.

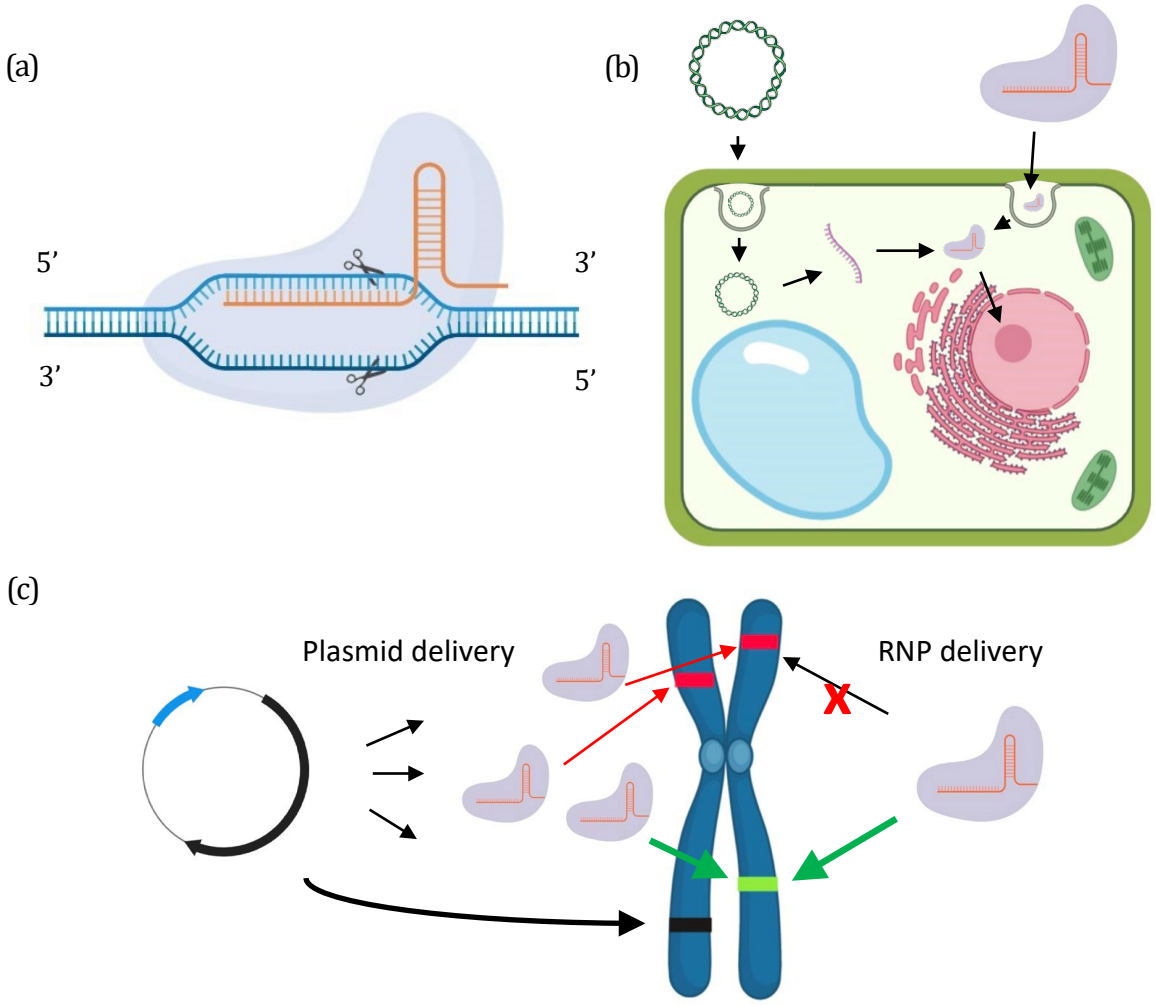

Figure 2: Genome editing with CRISPR-Cas9. (a) Structural schematic of Cas9 (blue, background) and single-guide RNA (orange) in complex with a DNA target molecule (blue, foreground). Double-stranded break cut site is indicated by scissors. **(b)** CRISPR genome editing in plants requires that exogenous biomolecules such as a plasmid (green helix) or preassembled RNP (purple/orange) bypass the plant cell wall (light green border) and cell membrane (dark green border), wherein the expression or direct delivery of Cas9 RNP is then followed by trafficking to the nucleus. **(c)** Plasmid delivery risks transgenic integration (black) and results in overexpression of Cas9 RNP, potentially leading to off-target cleavage (red). RNP delivery reduces the intracellular titre and expression duration of intracellular RNP, thus maintaining an optimal protein level sufficient for on-target cleavage (green) only.

4. The Complexities of Biomolecular Delivery to Plants

Intracellular delivery of large biomolecules such as proteins, DNA and RNA to plants has presented a massive bottleneck in the adaptation of modern biotechnological tools by plant scientists. To frame the problem, we consider that a plant's physical structure is dominated by a complex polymeric matrix known as the cell wall that acts as a near-impermeable barrier around each plant cell and, more broadly, prevents diffusive transport of large molecules into and throughout plant tissue. The plant cell wall is unique compared to bacterial or fungal cell walls in both its chemical composition (mostly cellulose, hemicellulose, and lignin) and in that it plays a critical role in maintaining structural integrity within a macroscopic organism. From one perspective, plants may be considered relatively closed physical systems apart from a few highly regulated inputs necessary for survival, e.g. photosynthetic inputs (sunlight and CO_2), water, soil micronutrients, and mycorrhizal symbiosis products. Inaccessibility of the plant intracellular space, and thus the challenge of delivering exogenous biomolecules to plants, is emphasized by considering that evolution has not generated a "passive" method for exogenous biomolecules to bypass the plant cell wall. Infection by plant pathogens (e.g. *Agrobacterium tumefaciens)* is largely mediated through injury to the plant cell wall by weather/animals or through complex secretory pathways and penetrative structures generated by microbial pathogens. However, recent research suggests that certain engineered nanomaterials (ENMs) are internalized by walled plant cells, presenting an opportunity for their use as biomolecule delivery vessels in plants. While the mechanism of internalization by ENMs to walled plant cells is unclear, their high charge density and small size (<10 nm) are hypothesized to be critical characteristics. Diffusion throughout plant tissue is limited by particle size such that passive particle transport through the cell wall polymeric matrix may be completely inhibited above a certain particle size. This so-called cell wall size exclusion limit varies based on host species, particle size, and surface chemistry but is generally reported on the order of 10-20 nm.

Developing improved strategies for bypassing the plant cell wall using ENMs is in part hindered by the challenge of visualizing local transport of molecules in the extracellular space. To date, most studies claiming to observe ENM internalization by walled plant cells have relied on confocal fluorescence microscopy. In this type of experiment, fluorescent signal from an exogenously introduced target molecule (e.g. a fluorophore-labeled ENM) is colocalized to morphological features or an endogenous fluorescent signal and taken to suggest cellular internalization. However, this strategy presents two issues. Absent of specialized techniques such as super-resolution imaging, confocal fluorescence microscopy is diffraction-limited to ~200 nm resolution considering that visible-range emitters are the most used fluorophores in cellular imaging. Cytosolic space within a plant cell is typically extremely thin and pressed against the plasma membrane due to turgor pressure exerted by the vacuole which, when coupled with the resolution limits of confocal fluorescence microscopy, makes intracellular and extracellular space difficult to distinguish. Secondly, fluorescence emission from endogenous plant pigments (i.e. autofluorescence) often exhibits significant spectral overlap with synthetic fluorophores used for imaging and

presents a high risk of detecting false positives without restrictive wavelength collection modes or spectral deconvolution methods. Detecting ENM internalization by non-optical methods such as electron microscopy can be useful for some ENMs with sufficient electron diffraction for imaging (e.g. gold nanoparticles[26]) but is not possible with many classes of non-diffracting ENMs that are of great interest (e.g. polymer nanoparticles, carbon nanotubes).

4.1. Agrobacterium and Biolistic Delivery

The current biomolecular delivery workhorses for genetic engineering in plants are *Agrobacterium* mediated transformation and biolistic particle bombardment. The *Agro* delivery method is a form of protein-assisted DNA transfer in which a bacterial plant pathogen, *Agrobacterium tumefaciens*, expresses a complex set of gene products in order to shuttle a linear fragment of bacterial DNA (known as the T-DNA) into the host nucleus and insert it into the host genome. The T-DNA can be engineered *in vitro* to contain genes of interest which would, upon integration, be expressed constitutively in the host cell. The advantage of *Agrobacterium* delivery lies in the highly efficient protein-assisted DNA transfer process, which typically results in efficient transformation and strong expression. However, *Agrobacterium* delivery is strictly limited to DNA cargo and stable integration, which presents substantial regulatory barriers in the United States due to the classification of transgenic plants as GMOs, and worldwide due to polarized attitudes and highly dynamic legislation surrounding genetically engineered crops (Figure 1). In the case of CRISPR-based genome editing using *Agrobacterium,* wherein an integrated CRISPR vector might target an endogenous gene transiently until a mutation abolishes the target sequence, the transgenic elements often must be segregated out using traditional breeding techniques. In addition, *Agrobacterium* transformation exhibits substantial host range limitations due to the limited number of plant species that can be infected by laboratory strains of *Agrobacterium*.

Biolistic particle bombardment is a form of mechanically-assisted cargo transfer in which biomolecules are dehydrated onto the surface of a gold particle ~600 nm in diameter and loaded into a device (known as a gene gun) pressurized to 100-500 psi with helium gas. The loaded particles are then ejected from the device at high pressure and allowed to penetrate a tissue sample. Thus, bombardment provides a means for exogenous cargo to forcibly enter the cell and may result in transient expression, although stable transformation with biolistics is also a common application. Severe mechanical disruption of the cell may in genomic shearing and subsequent chromosomal repair results in the integration of genetic cargo into the host genome. Compared to *Agro*, biolistic delivery exhibits less tissue and species specificity as the method of entry is entirely mechanical. However, shearing of DNA cargo may result in random fragment integration and thus biolistic delivery is similarly subject to regulatory barriers related to transgene integration. As proteins can also be loaded onto particle carriers, biolistic bombardment is not theoretically limited to DNA delivery, although the moisture-free gaseous environment inside of a gene gun may promote protein unfolding and subsequent loss of cargo function. Examples of biolistic protein delivery do

exist in the literature (Table 2), although low transformation efficiencies emphasize the challenges of this method.

Additional methods of biomolecule delivery in plants include polyethylene glycol (PEG) transfection, electroporation, and cell-penetrating peptide (CPP) mediated delivery. PEG transfection involves the enzymatic degradation of cell wall to form protoplasts, or singly suspended unwalled plant cells, and PEG-assisted transfer of biomolecules across the plasmid membrane. While PEG transfection is efficient, amenable to DNA, RNA, and proteins, and does not result in host integration, the primary limitation lies in regeneration of protoplasts after transfection. Protoplast regeneration back into whole, cell-walled plants by tissue culture methods remains a difficult challenge for a wide variety of plant species and so PEG transfection is best suited for transient gene expression studies.

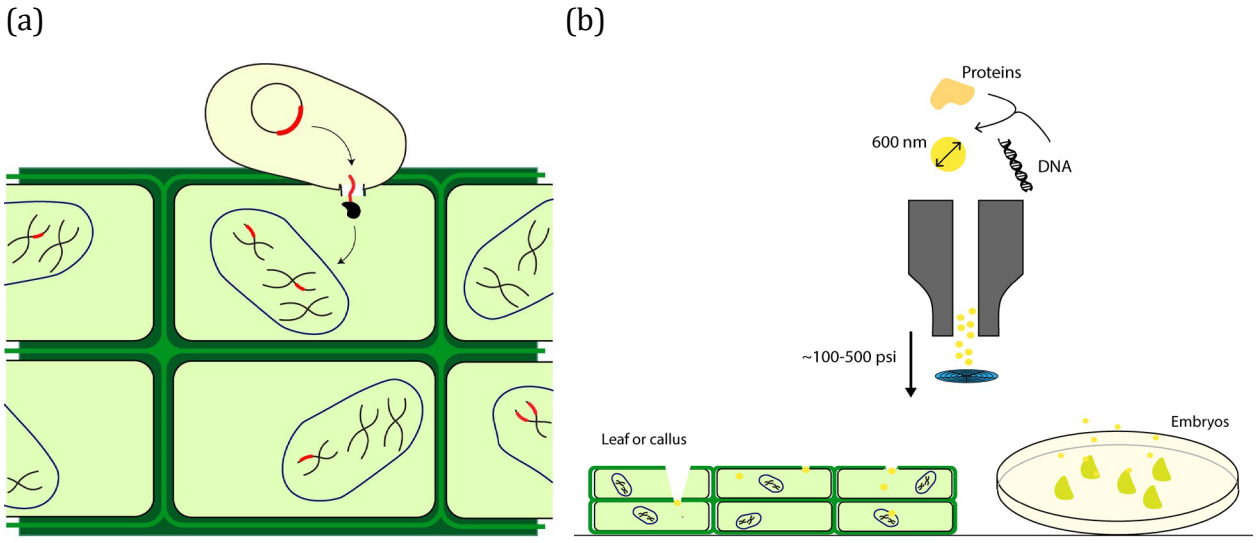

Figure 3: Traditional biomolecule delivery methods in plants. (a) *Agrobacterium*-mediated transformation hijacks bacterial machinery to incorporate a synthetic DNA cassette into the host genome via a complex protein-mediated integration mechanism. **(b)** Biolistic transformation utilizes a high pressure device known as a gene gun to launch biomolecular cargo adsorbed to gold microparticles into plant tissue. Mechanical disruption of the cell allows for integration of synthetic DNA into the host genome or delivery of active proteins to the intracellular space.

4.2. Nanoparticle-mediated delivery

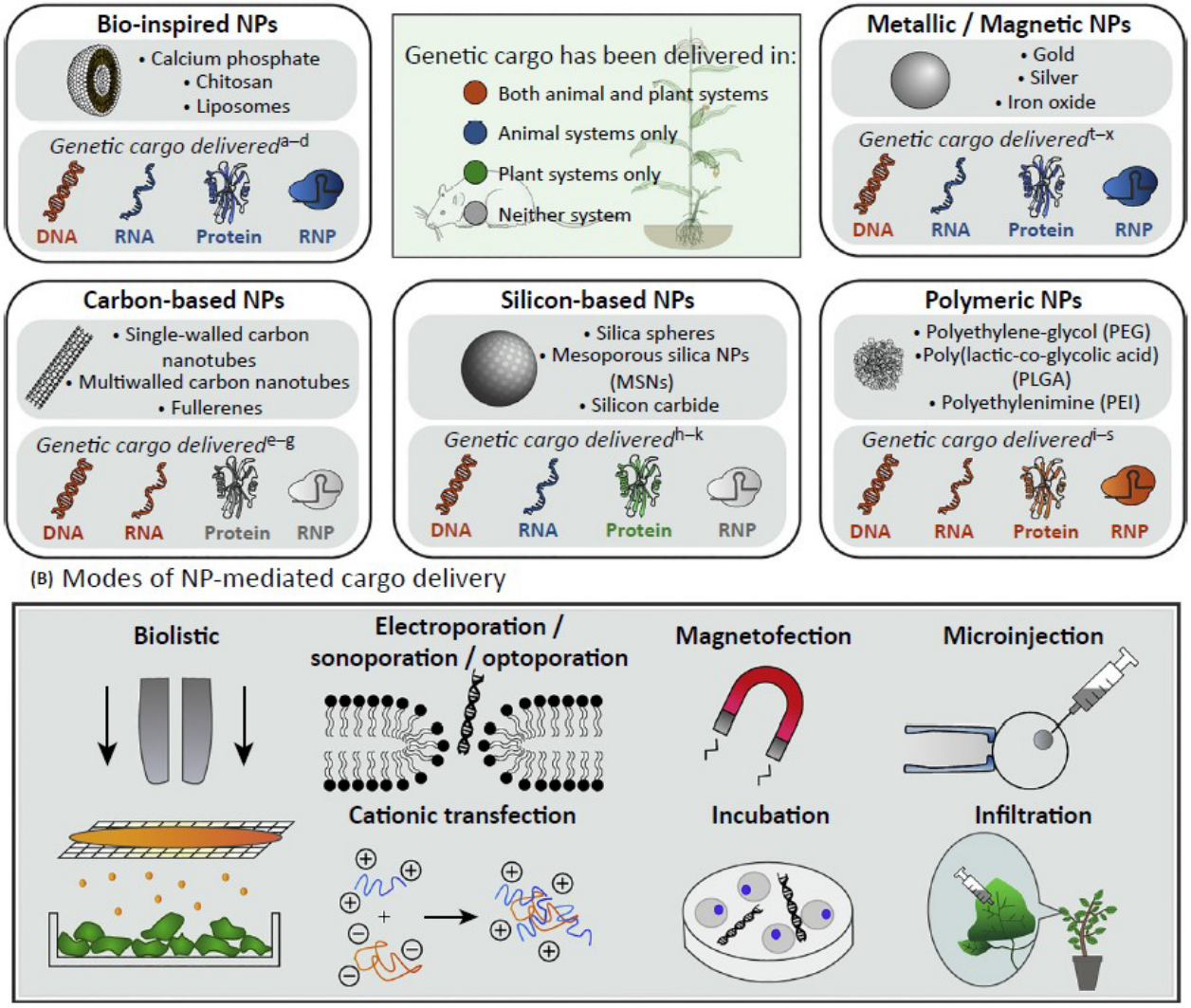

Figure 4: Overview of nanoparticle delivery methods in animal and plant systems. Adapted with permission.[3]

In the interest of developing additional tools for plant transformation that mitigate common pitfalls of current techniques, our lab has put forth an effort to develop nanomaterial-based strategies for biomolecule delivery to plants that addresses several challenges: efficient delivery of functional cargo without host integration (i.e. transient expression), tissues/species independence, and a diversity of cargo loading capabilities. Nanomaterials are promising candidates towards addressing these challenges, owing to their ability to apparently traverse the numerous barriers to intracellular delivery, namely the cell wall, cell membrane, and intracellular membranes. Nanoparticle (NP) size is typically defined as <100 nm in at least one dimension, although in this work we focus on NPs <20 nm

as these smaller NPs have so far shown the greatest success for plant cellular delivery. In addition to size, NP surface chemistry is also a key characteristic of uptake as well as an opportunity to tune NP affinity based on cargo. Manipulating NP surface chemistry could also enable secondary functions that direct localization, uptake, and release properties *in vivo*.

To date, a modest number of studies have demonstrated promising success for nanoparticles as delivery tools in plants (Table 3). Early examples of plant nanoparticle delivery used gold-capped mesoporous silica nanoparticles (MSNs) in combination with a gene gun for delivery of DNA and proteins to tobacco, maize, and onion[27–29] – in these studies, MSN pores were used for cargo loading, while the conjugated gold particle and gene gun remained as the components responsible for internalization into tissue. Organic functionalization of MSNs has been found, in one study, to enable passive internalization in *Arabidopsis thaliana* roots for transient expression without external aid.[30] Other nanoparticle systems used in the literature for passive delivery to mature plants include poly-L-lysine coated starch nanoparticles[31], magnetic Fe3O4 nanoparticles[32], polyamidoamine dendrimers[33,34], calcium phosphate nanoparticles[35], and layered double hydroxide clay nanosheets[36] – however, there lacks a consensus on which nanoparticle system is the most efficient, widely applicable, and reproducible.

5. Covalent Polymer-SWNT Conjugates for Plasmid Delivery

Single-Walled Carbon Nanotubes (SWNTs) are an example of one ENM that has shown success as a biomolecular carrier in walled plant cells. Our lab has developed a polyethyleneimine-functionalized SWNT material (PEI-SWNT) for DNA delivery to leaves, wherein negatively charged plasmids are electrostatically bound to cationic PEI-SWNTs (Figure 5a)[37]. In this study, a fluorescent reporter (GFP) was expressed by PEI-SWNT mediated transformation in *Nicotiana benthamiana* leaves, supported by confocal fluorescence imaging and molecular data (quantitative real-time PCR), as well as the agriculturally relevant species wheat, cotton, and arugula.

We then sought to explore whether PEI-SWNTs could be used to deliver DNA vectors with functional utility in the plant science community, i.e. plasmids encoding CRISPR-Cas9 machinery. To this end, we designed a set of CRISPR plasmids targeting GFP expressed constitutively in a *N. benthamiana* stable transgenic line (Figure 7a). As gene editing efficiency is known to be correlated to sgRNA sequence, we designed and screened three candidate sgRNAs targeting locations in the mGFP5 transgene that, based on a BLAST query, contained no off-target hits in the wildtype *N. benthamiana* genome. These sgRNA sequences were cloned into a plasmid backbone containing Cas9 such that the final vector contained both elements necessary for CRISPR editing. Promoter selection was based on choosing appropriate drivers for strong expression of protein (CaMV 35S) and non-translated RNA (AtU6-26), which are driven by different RNA transcriptase proteins in plants (RNAP II and RNAP III for mRNA and snRNA, respectively). The sgRNA expression cassette also contains a poly-T terminator (T6) to efficiently terminate RNAP II transcription at the 3' end of the scaffold region and maximize proper sgRNA folding *in vivo*. Upon successful construction of

three CRISPR vectors targeting unique regions in transgenic GFP, we formed DNA-PEI-SWNT complexes by coincubation and assayed functionality *in vivo* by needleless syringe infiltration to transgenic *N. benthamiana* leaves followed by isolation of genomic DNA and PCR amplification of the GFP target locus (Figure 6). Genomic amplicon pools, containing a mixture of unmutated and mutated sequences, were Sanger sequenced and indel frequency was analyzed by inputting Sanger chromatograms into the Tracking Indels by DEcomposition (TIDE) algorithm. TIDE is used to measure indel frequency through a statistical decomposition method that compares chromatographic signals between control and experimental groups to detect indels and their relative frequency in the total pool of amplicons.[38] While TIDE lacks the sensitivity of more advanced methods that utilize Next-Generation Sequencing data to detect CRISPR-induced mutations, its advantage lies in its simplicity and speed as no library preparation is required and Sanger sequencing services are readily available with quick turnaround times.

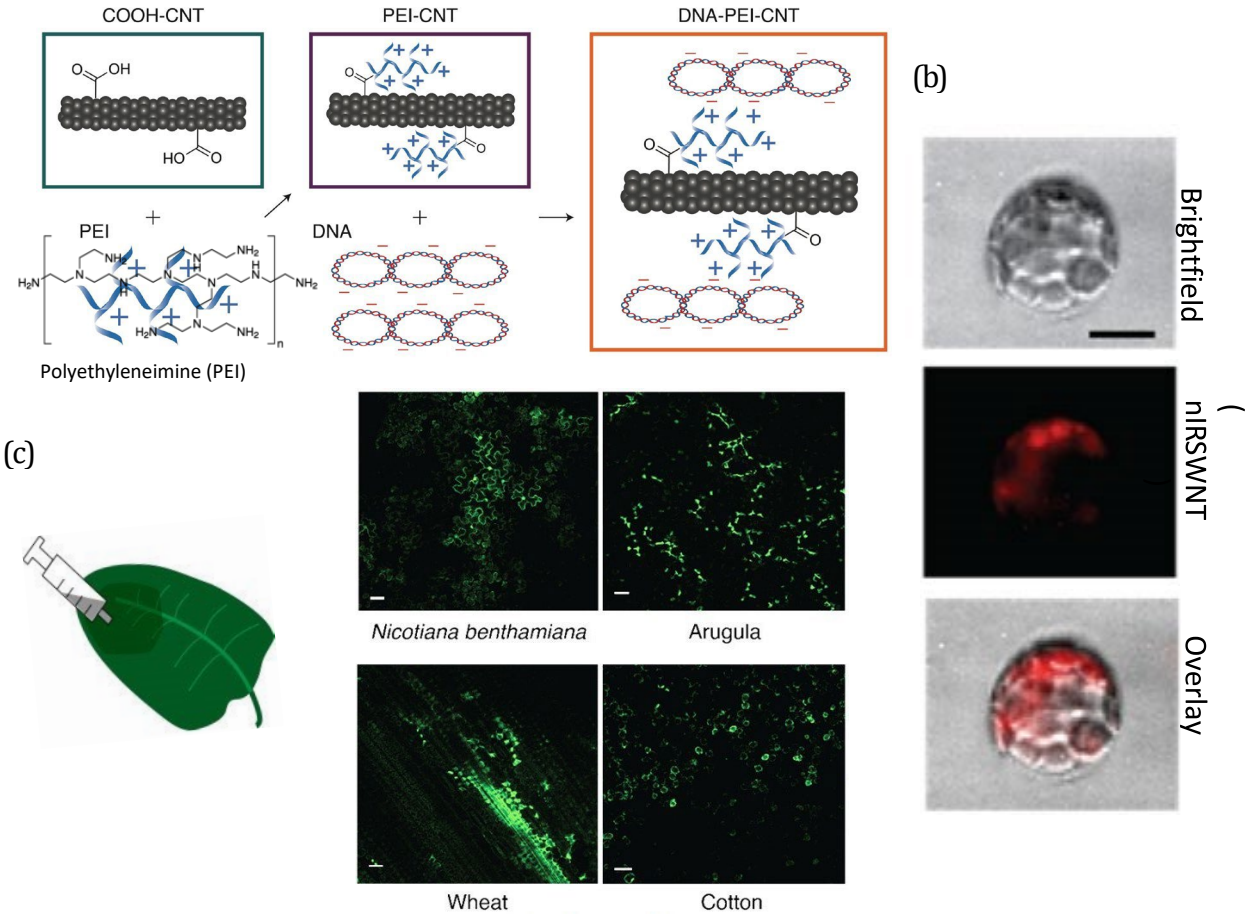

Figure 5: Polymer-SWNT conjugates for plasmid delivery to leaves. (a) Noncovalent electrostatic adsorption of DNA to SWNTs (also known as CNTs) is enabled by covalent attachment of a cationic polymer, polyethyleneimine, to pristine SWNTs containing amine-reactive carboxyl groups. **(b)** Widefield fluorescence microscopy of *Nicotiana benthamiana* protoplasts demonstrates cellular uptake of DNASWNTs as shown by colocalization of cells and intrinsic near-infrared SWNT fluorescence. **(c)** Confocal fluorescence microscopy of leaves infiltrated with PEI-SWNTs complexed to a plasmid encoding for GFP. Transient GFP

expression fluorescence is demonstrated in the leaves of dicot (*Nicotiana benthamiana,* arugula) and monocot (wheat, cotton) plant species. Adapted with permission.[37]

To motivate CRISPR RNP delivery as the main focus of this work, we point out that current formulations of plasmid-PEI-SWNTs result in lower expression compared to *Agrobacterium*-mediated delivery[37], potentially due to high toxicity of PEI[39] or tight condensation of plasmids onto PEI-SWNTs which minimizes access by transcriptional machinery.[40] Coupled with the regulatory barriers associated with DNA delivery to plants, it is of great interest to accelerate development of protein delivery strategies using ENMs, an area which is particularly understudied.

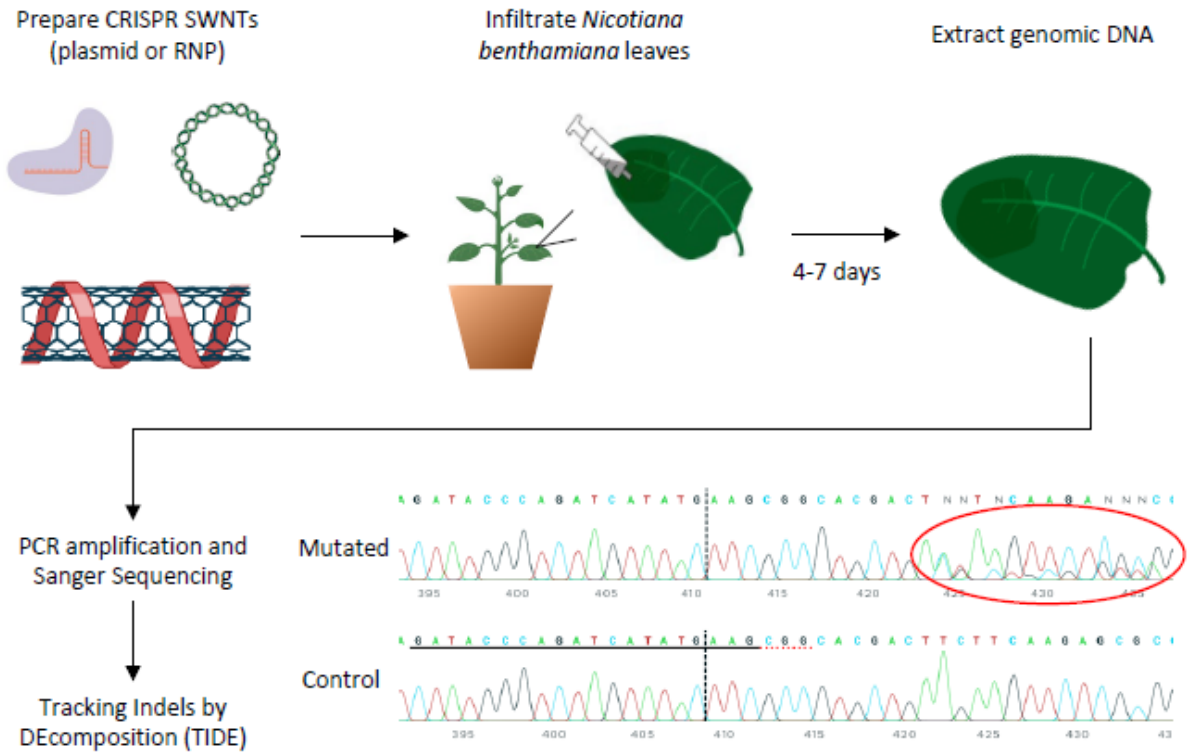

Figure 6: Workflow for assaying SWNT-mediated CRISPR-induced mutations. CRISPR-SWNTs are prepared by complexing a CRISPR plasmid vector to PEI-SWNTs, or through association of preassembled Cas9 RNP with functionalized SWNTs. Upon leaf infiltration, CRISPR expression and genomic targeting is allowed to proceed for several days before genomic DNA is extracted. The target locus is then amplified by PCR and analyzed by Sanger Sequencing. Using the TIDE algorithm, sequence chromatograms of amplicons from CRISPR-SWNT infiltrated leaves are statistically analyzed against a control (unmutated) leaf to calculate the percentage of PCR amplicons containing an insertion or deletion mutation (indels). In the example control chromatogram, the sgRNA target sequence is underlined in black, the PAM sequence is underlined in a red dotted line, the cut site is indicated with a black dotted line. In the example chromatogram containing mutations, a region downstream of the cut site with high sequence uncertainty is circled in red, indicating the presence of a mixed pool of mutated and unmutated amplicons.

5.1 PEI-SWNT Synthesis

Polyethyleneimine-SWNT conjugates are prepared using EDC/NHS carbodiimide crosslinking as previously described[41]. First, a carboxylated SWNT slurry is prepared in water at 1 mg/mL by bath sonication for 10 minutes followed by probe tip sonication for 30 minutes at ~30-40 W. The slurry is allowed to cool to room temperature before centrifugation at 18,000xg for 1 hour. The supernatant, containing suspended carboxy-SWNTs, is collected and the SWNT concentration determined by absorbance at 632 nm (ε = 0.036 L mg^{-1} cm^{-1}). The carboxy-SWNT suspension may be stored at 4 ^{o}C and used for multiple conjugation reactions. 2 mg of carboxy-SWNT are added to MES buffer, pH 4.5, such that the final concentration of MES is 100 mM. A fresh solution of EDC/NHS is prepared at 4 mg/mL of each component in 100 mM MES pH 4.5. The EDC/NHS solution is then added dropwise to the carboxy-SWNT suspension while stirring, and bath sonicated for 15 minutes. The reaction, which generates amine-reactive esters on the SWNT surface, is allowed to continue on an orbital shaker at room temperature for 1 hour. Upon completion, the activated carboxy-SWNTs are washed 3x with 0.1X PBS via spin filtration through a 100kDA MWCO cellulosic membrane. After 3 washes, the filter cassettes are removed from the flowthrough tube and bath sonicated to recover activated COOH-SWNT precipitates from the membrane. The activated COOH-SWNT suspension is then recovered and diluted to the initial reaction volume in 0.1X PBS followed by bath sonication for 10 minutes. Meanwhile, 40 mg of 25kDa branched polyethyleneimine (PEI) is prepared in 0.1X PBS and corrected to pH 7.4 using HCl. The activated COOH-SWNTs are then added to the PEI solution dropwise and the amination reaction is allowed to proceed overnight on an orbital shaker. It may be necessary to readjust the pH of the reaction solution to 7.4 as the solution will become alkaline as the reaction proceeds. This amination reaction links PEI to the SWNT surface via cleavage of the active ester intermediate. Upon completion, crude PEI-SWNT is washed 6x with water by spin filtration through a 100K MWCO cellulosic membrane, with aggregates recovered by bath sonication of the filter cassette. The filtered PEI-SWNTs are then recovered and diluted to the original volume of suspended carboxy-SWNTs added to 100 mM MES. This suspension is then probe tip sonicated for 15 minutes (30-40 W) and centrifuged for 1 hour at 16,000xg. The supernatant is collected and SWNT concentration measured via absorbance at 632 nm (ε = 0.036 L mg^{-1} cm^{-1}).

5.2 Plasmid Delivery *in planta*

Extending the PEI-SWNT plasmid delivery platform to include DNA vectors with functional utility in the plant biotechnology community, we sought to explore PEI-SWNT mediated delivery of a CRISPR plasmid vector targeting chromosomal GFP in a transgenic line of *N. benthamiana*. As discussed in the CRISPR Methodology section, we designed three sgRNA targets and cloned them into individual plasmid vectors containing expression cassettes for both sgRNA and Cas9. Infiltration of PEI-SWNTs complexed to plasmid DNA encoding CRISPR machinery targeting the mGFP5 transgene in *Nicotiana benthamiana* leaves resulted in the introduction of indel mutations at the target locus, as measured by

TIDE. When 1 ug of total plasmid is delivered to the leaf, the mutation frequencies are 2.6 ± 0.05 %, 5.5 ± 1.1 %, and 3.4 ± 0.05%, for g206, g207, and g208 target sites, respectively, measured from genomic DNA isolated from the entire infiltration area (Figure 7c). We note that the detection threshold in these experiments, as determined from a buffer infiltrated control leaf, was approximately 1%. We hypothesized that the mutation frequency, and thus our confidence in the results as being sufficiently above noise, could be increased by increasing the total plasmid dosage to 2.5 ug. To that end, we observed a positive dose response with respect to total plasmid delivered: when 2.5 µg plasmid is delivered to the leaf, mutation frequencies in the entire infiltration area increase to 5.2 ± 0.25 %, 8.5 ± 0.54 %, and 4.8 ± 0.28%, for g206, g207, and g208 target sites, respectively. Furthermore, the measured mutation frequency increased to 15.3% (2.5 ug g208) when isolated to a small section of leaf tissue adjacent to the infiltration site, suggesting that effective plasmid dosage diminishes throughout the leaf tissue likely due to inhibited diffusion of PEI-SWNTs through the cell wall. We point out that while mutation frequencies within 5-20% are not unusual for *Agrobacterium* and biolistic-mediated delivery of CRISPR vectors to plants, PEI-SWNTs do not possess an intrinsic advantage for CRISPR plasmid delivery as far as delivery efficiency is concerned. However, the broader range of species compatible with PEI-SWNT plasmid transformation makes them a viable alternative option to researchers interested in exploring alternative delivery modalities for their CRISPR workflows.

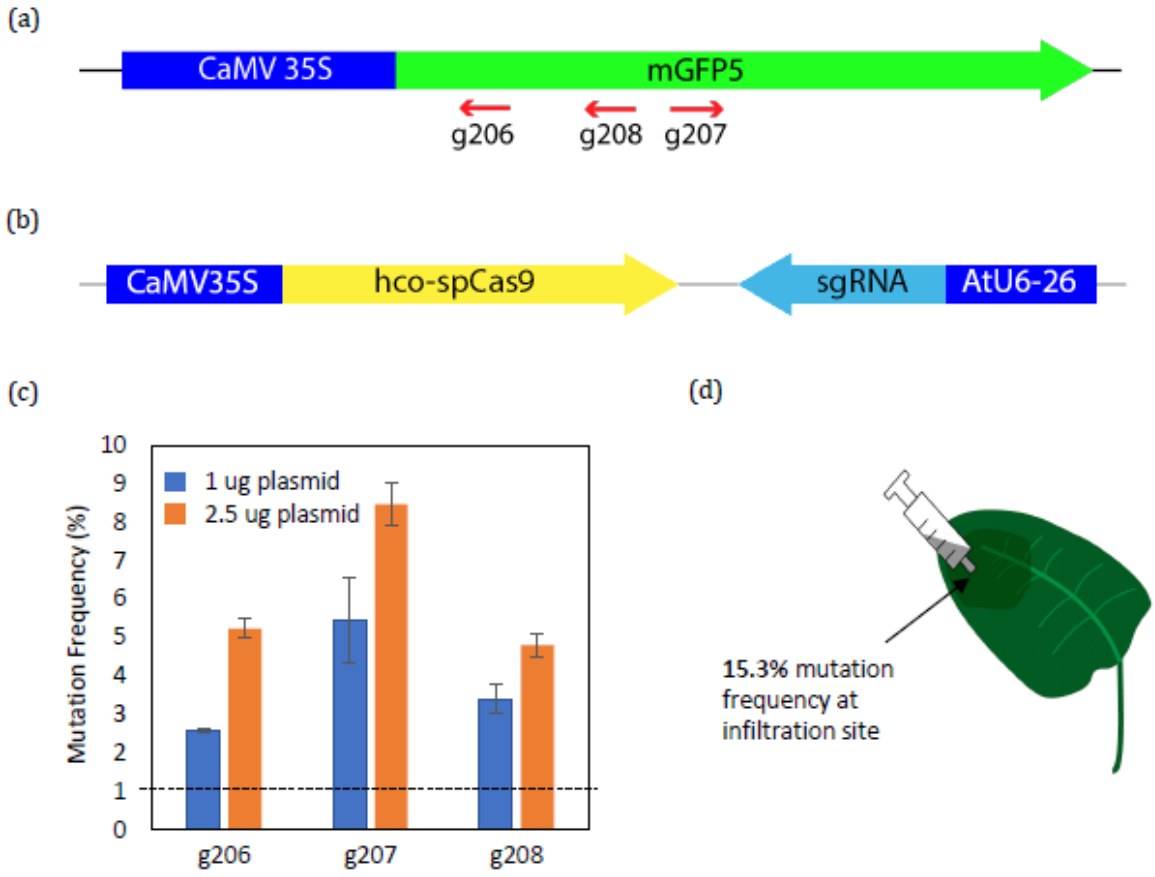

Figure 7: CRISPR plasmid delivery by PEI-SWNTs. (a) Transgene schematic for GFP-expressing *Nicotiana benthamiana.* Constitutive mGFP5 expression in *N. benthamiana*

tissue is driven by the Cauliflower Mosaic Virus 35S promoter (*CaMV 35S*). Target locations for three independently designed sgRNAs (g206, g207, g208) are indicated by red arrows. **(b)** Gene schematic for 9.5 kbp CRISPR plasmids used in this study. Human-codon optimized Cas9 from *Streptococcus pyogenes* is driven by the *CaMV 35S* promoter. sgRNA expression is driven by a small nuclear RNA promoter, U6-26 from *Arabidopsis thaliana* (*AtU6-26).* **(c)** Mutation frequency (TIDE) for *N. benthamiana* leaves infiltrated with CRISPR DNA-PEISWNTs containing variable amounts of total plasmid. Amplicon pools were derived from total extracted genomic DNA in the entire infiltration area. Dotted line indicates TIDE noise threshold. **(d)** Mutation frequency as measured by TIDE for genomic DNA sample extracted close to the infiltration origin site (< 2 mm from infiltration wound). Data shown for g208 target at 2.5 ug plasmid.

6. DNA-Free Genome Editing

Most examples of CRISPR genome editing in plants rely on transient or stable expression of editing machinery through delivery of a DNA vector expressing both components of the CRISPR system, e.g. Cas9 and sgRNA. There is, however, a strong motivation to develop 'DNA-free' methods for genome editing via direct delivery of preassembled ribonucleoproteins (RNPs). Plasmids or integrated cassettes tend to overexpress a gene of interest for days to weeks and sustained high concentrations of RNP within a cell can lead to toxicity or off-target cleavage. We point out that vector improvement using 'design-build-test' strategies applied to promoter, CDS, and terminator optimization could be useful for tuning intracellular titre of RNPs expressed from exogenous DNA, but large vector libraries for plants remain in early development and characterization stages. In contrast, RNP delivery has been shown to reduce off-target indels in comparison to RNP expression from a delivered plasmid through tighter control of RNP concentration and cellular half-life.[42] Importantly, RNP delivery also abolishes all risks of transgene integration, therefore eliminating potential genomic destabilization caused by sustained nuclease overexpression and getting rid of the need to segregate transgenes out of future generations. Furthermore, as transgenic plants introduce regulatory burdens due to their classification as GMOs in the United States, any plant cultivar that has been engineered using a DNA vector is subject to the long and tedious process of regulatory review, even if the vector is meant to be non-integrating. While some examples of RNP delivery exist in the literature (Table 2) they are limited in scope and efficiency due in part to a lack of efficient delivery tools, thus illustrating the need for novel protein delivery conjugates.

7. Colloidal Design of Protein-ENM Pairs

A primary focus of this work is exploring the potential of ENMs as protein delivery vessels in plants, which to date has fewer example cases in the literature compared to ENMs

for nucleic acid delivery. Considering the wide breadth of relatively shallow literature on many ENM-protein systems, the design space for protein-nanomaterial pairs with novel applications and enhanced delivery efficacy is massive and, depending on the researcher's goals and background, is often approached in various ways that prioritize a certain class of ENM or a certain protein cargo. However, major challenges arise in part from the complex colloidal nature of most ENM delivery systems. Understanding dispersive interactions within colloidal nanoparticle-protein conjugates is essential to designing an effective delivery formulation. However, colloidal behavior is difficult to broadly predict by chemical/structural design alone due to the inherent thermodynamic instability of colloids - systems of particles defined by a balance between weak and strong forces of repulsion and attraction. Thus, a given colloidal state is tightly linked to process as well as formulation and may evolve significantly over time or be highly sensitive to factors not easily controlled across different laboratories, such as instrumentation or reagent sources. Furthermore, the lack of a unified approach to designing colloidal nanomaterial carriers for a specific application often forces researchers to synthesize distantly related structural and functional data associated with individual components of a delivery conjugate to inform a theoretical design strategy from which to start testing. In the case of ENM-mediated CRISPR protein delivery, it is useful to first consider the available structural information that sheds light on forces governing colloidal and functional stability of the Cas9 enzyme.

Native state apo-Cas9 is multiconformational and characterized by substantial flexibility especially within catalytically active domains of the protein when not complexed with sgRNA[43]. However, upon binding an sgRNA molecule, Cas9 RNP undergoes a dramatic conformational change to a highly stable state that structurally primes the target recognition and cleavage domains.[44] In addition, the high molecular weight of Cas9 (160 kDa, ~10 nm) may lead to protein-protein aggregation, a commonly observed phenomena of large proteins under many conditions. Like many colloidal systems, Cas9 solubility is enhanced at increased charge densities, which allows for engineered stabilization of Cas9 through the introduction of ionic stabilizers such as synthetic cationic[45] or anionic[46] polymers. We point out that apo-Cas9 has a measured zeta potential of +5 to 10 mV while Cas9 RNP assumes a negative zeta potential of -5 to 10 mV, further emphasizing the ambiguous role that charge identity can play in engineered stabilization of protein-ENM colloids. Interestingly, Cas9 RNP stabilization by ionic polymers extends even to the point of improved editing outcomes, suggesting that the mechanism for continued stabilization *in vivo* may be far more complex than what can currently be described by colloidal theory of simple systems.

8. Cas9 Fusion Proteins for Direct Adsorption to SWNTs

As proteins are known to nonspecifically associate with the SWNT surface absent of a ligand-specific interaction[47], we investigated the utility of Cas9 to suspend SWNTs by ultrasonication. Purified Cas9 was found to be a moderate dispersant of pristine SWNTs (Figure 8a) likely through nonspecific interactions between hydrophobic residues on Cas9 and the nonpolar SWNT surface. However, sonication was found to completely abolish Cas9

enzymatic activity *in vitro* (Figure 8b), suggesting that harsh conditions of sonication might cause protein unfolding and subsequent deactivation. Thus, we reemphasize the need for an intermediate ligand to bind Cas9 to SWNTs upon coincubation of preassembled RNP and suspended nanotubes. In contrast to designing a SWNT ligand that binds wildtype Cas9, an alternative strategy towards the development of a Cas9-SWNT conjugate is to genetically fuse SWNT-binding elements to the Cas9 protein. Upon recombinant expression and purification of Cas9 fused to a SWNT-binding domain, one could then form protein-SWNT conjugates using an orthogonal SWNT dispersant, such as ssDNA which is known to suspend SWNTs with high yield and prolonged stability. To this end, we designed and tested two Cas9 fusions for direct binding of Cas9 to the SWNT surface.

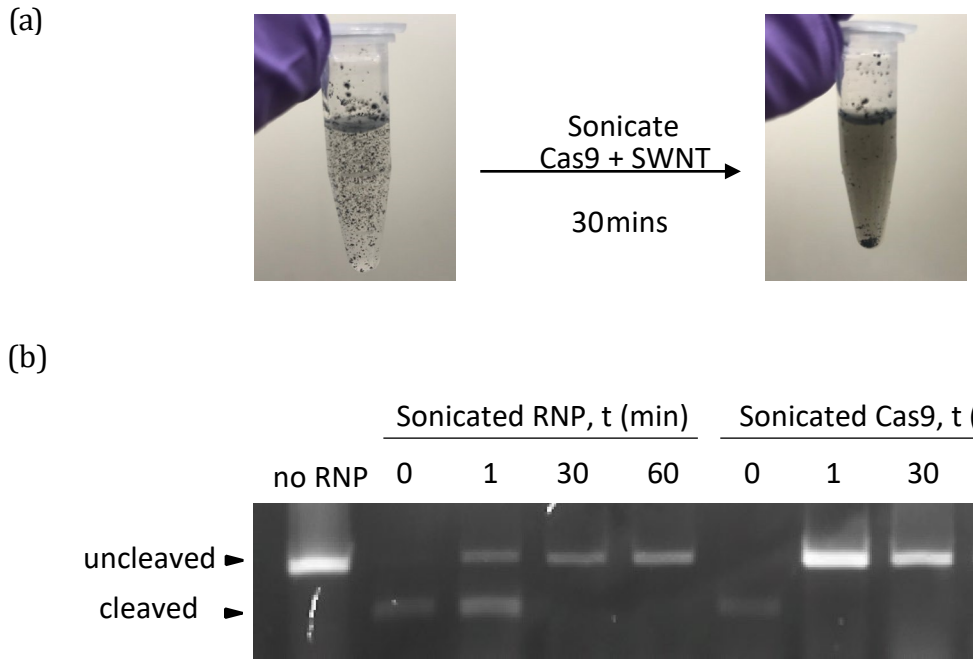

Figure 8: Direct adsorption of Cas9 to SWNTs by sonication. (a) Coincubation and ultrasonication of SWNTs and Cas9 results in a semi-stable SWNT suspension (right) indicated by a visual transition to a homogenous grey suspension upon sonication. **(b)** Sonication of RNP or Cas9 abolishes enzymatic function as demonstrated by a Cas9 *in vitro* cleavage assay. Presence of a cleaved band indicates Cas9 enzymatic activity while the uncleaved band suggests loss of enzymatic function.

The first Cas9 fusion design strategy made use of the streptavidin-biotin system, a naturally occurring ligand pair with one of the strongest non-covalent interactions known in nature. Streptavidin is a tetrameric 60 kDa protein that cooperatively binds biotin[48], a small molecule with a nitrogen- and sulfur-containing heterocycle, with a dissociation constant on the order of 10^{-14} mol/L[49]. Applying the streptavidin-biotin system for SWNT

functionalization starts with covalent attachment of biotin to the SWNT surface via nucleophilic substitution of triazine-functionalized SWNT by amine-conjugated biotin[50]. The resultant covalently functionalized nanotubes are thus 'biotinylated' and are primed for decoration with a streptavidin ligand, in this case Cas9 fused to streptavidin. However, the nearly irreversible tetrameric streptavidin binding complex presents two issues for its application in a Cas9-SWNT system for plant cellular delivery. First, Cas9's large size (160 kDa) and the tetrameric nature of bound streptavidin introduce steric considerations that could prevent complex formation altogether or risk SWNT colloidal destabilization due to the formation of a large multimeric protein assembly on the SWNT surface. Second, the extremely high affinity of streptavidin to biotin is somewhat hindering in a delivery context, where release of protein cargo from its carrier into the intracellular space is ultimately desirable. Taking sterics and affinity into consideration, we designed a Cas9 fusion using an engineered form of streptavidin, monoavidin, that binds biotin monomerically with a increased dissociation constant of 10^{-7} mol/L[51]. While we were able to show that biotinylated SWNTs can bind Cas9-monoavidin, the conjugate was only stable at reduced temperature (4 ^{o}C) and was therefore not pursued any further for delivery applications in plants.

The second Cas9 fusion design strategy utilized a small peptide with affinity to the SWNT surface. A carbon nanotube-binding peptide (CBP) with amino acid sequence HWKHPWGAWDTL was previously identified using phage display to have selective affinity for carbon nanotubes[52]. CBP binding affinity is related to an enrichment of aromatic and hydrophobic residues as well as a flexible fold that complements the geometry of carbon nanotubes. We sought to leverage CBP-SWNT affinity to promote adsorption of Cas9 to SWNTs through genetic fusion of Cas9 and CBP followed by recombinant expression and purification. Cas9-CBP fusion protein was designed to also contain an SV40 NLS to ensure nuclear accumulation upon cellular delivery, as well as a flexible GGS linker to minimize structural crosstalk between Cas9 and the peptide elements NLS and CBP (Figure 9a).

9. SWNT-mediated RNP delivery by Cas9-CBP fusion protein

A summary of results for the Cas9-CBP fusion protein delivery strategy is shown in Figure 9. We first sought to characterize the colloidal stability of Cas9-CBP in complex with ssDNA suspended SWNTs using Dynamic Light Scattering (DLS), which measures the temporal scatter profile of an incident laser to estimates the hydrodynamic radius of a spherical particle with equivalent diffusivity to the protein-SWNT conjugate particle. The results for the DLS study of Cas9-CBP-SWNTs are shown in Figure 9b, where the hydrodynamic radius is normalized to DNA-SWNTs alone. The average particle radius is shown to be dependent on the ratio of Cas9:SWNT with a positive correlation, i.e. increasing particle size, at higher ratios of protein to SWNT. Normalized particle sizes relative to SWNTs are approximately 1x, 4x, and 12x for protein:SWNT ratios of 1:1, 10:1, and 100:1, respectively. However, DLS data alone does not provide information on the maximum number of proteins that can be stably loaded onto SWNTs, as aggregate formation cannot easily be distinguished from stable association by considering only the hydrodynamic radius. Atomic Force Microscopy (AFM) provides a means to directly visualize the colloidal state, i.e.

to infer the formation of stable, individually suspended conjugates versus large aggregates. AFM images of Cas9-CBP-SWNTs are shown in Figure 9d. AFM images reveal that at a 10:1 molar ratio of protein:SWNT, individually suspended SWNTs dominate the colloidal behavior of the system. However, at a 100:1 ratio of protein:SWNT, we observe the formation of large aggregates as seen through AFM. Thus, we conclude that the bulk molar ratio of protein:SWNT must be kept below 10:1 in order to maintain a stable suspension amenable for delivery.

We then assayed the ability of Cas9-CBP-SWNTs to induce mutations in the target gene, GFP, upon infiltration into a leaf of transgenic *N. benthamiana* constitutively expressing GFP. Results for indel frequency as measured by TIDE are shown in Figure 9c. A baseline detection threshold is first established by considering the calculated indel frequency, resulting from noise in the Sanger chromatogram, of a buffer-infiltrated leaf. For these experiments, the detection threshold was determined to be 0.54%. Cas9-CBP-SWNTs were found to induce mutations at 1.4% and 0.6% for a protein:SWNT molar ratio of 10:1 and 5:1, respectively. While a 1.4% mutation frequency for 10:1 protein:SWNT is slightly above the detection threshold, we conclude that more replicates are needed to increase confidence in these results. Furthermore, we suggest that a higher dosage of Cas9 could improve editing efficiency based on data collected from peptoid-RNP-SWNT infiltrations discussed in the following sections.

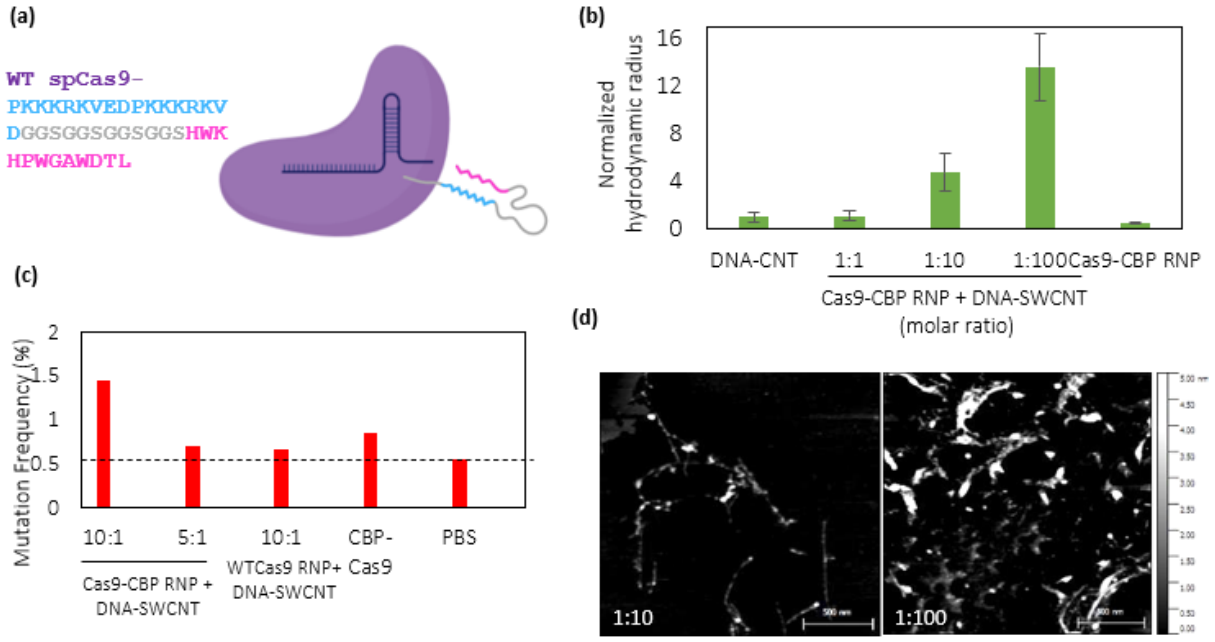

Figure 9: Cas9-CBP fusion protein for direct binding to suspended SWNTs. (a) Structural schematic indicating Cas9-CBP fusion protein design strategy containing: WT spCas9 (purple) fused to an SV40 nuclear localization sequence (blue), a flexible linker (grey), and a SWNT-binding peptide (pink). **(b)** Hydrodynamic radius of DNA-SWCNT and Cas9-CBP complex as measured by DLS. Normalized to DNA-SWNT radius. **(c)** Mutation frequency (TIDE) of leaves infiltrated with Cas9-CBP RNP DNA-SWCNT complexes, targeting

mGFP5 (g208) in transgenic *N. benthamiana* (N=1). Dotted line represents noise threshold. PBS = phosphate buffered saline. **(d)** Representative AFM images of Cas9-CBP RNP DNA-SWCNT complexes at varying molar ratio of protein:SWCNT.

10. Noncovalent Peptoid-SWNT Conjugates for Protein Delivery

Designing an appropriate SWNT surface chemistry for Cas9 protein conjugation and delivery presents significant challenges in maintaining protein stability and enzymatic functionality. Cas9 RNP activity was found to be inactivated in the presence of PEI-SWNTs (data not shown), thus the need for a novel chemistry to bind Cas9 to SWNTs was apparent. The high charge density of synthetic ionic polymers such as PEI, especially when concentrated on the SWNT surface, may play a role in Cas9 structural disruption. Compared to synthetic polymers, biopolymers such as oligonucleotides and peptides are often preferred for SWNT functionalization owing to their sequence-specific structural tunability and commercial availability. However, biopolymers are prone to enzymatic degradation, may be expensive to produce, and canonical synthesis methods are limited in their chemical diversity. Biomimetic polymers, in contrast, retain many of the advantages of naturally occurring biopolymers but are often developed with a strong emphasis on facile synthesis techniques and maximal chemical diversity. To this end, we identified peptoids, or poly-*N*-substituted glycines, as a biomimetic polymer with great potential as a novel protein-SWNT conjugate chemistry. Peptoids are sequence-defined synthetic polymers, typically 10-40 monomers in length, that are heavily inspired by peptides as evidenced by their chemical similarity (Figure 10a). Via a stepwise solid-phase submonomer synthesis method, peptoids are amenable to robotic synthesis with a large monomer space of primary amines that dictate functionality.[53] Peptoids are also resistant to protease degradation[54], making them ideal candidates as functional biorthogonal tools *in vivo*. SWNT functionalization with peptoids for protein conjugation is inspired by recent work in which self-assembling peptoid nanostructures were shown to be capable of specific multivalent interactions with kinases and lectins[55]. Our lab was the first to incorporate these nanosheet peptoids into self-assembling structures with SWNTs, demonstrating the ability of SWNT-peptoid conjugates to selectively recognize a lectin protein known as Wheat Germ Agglutinin[56].

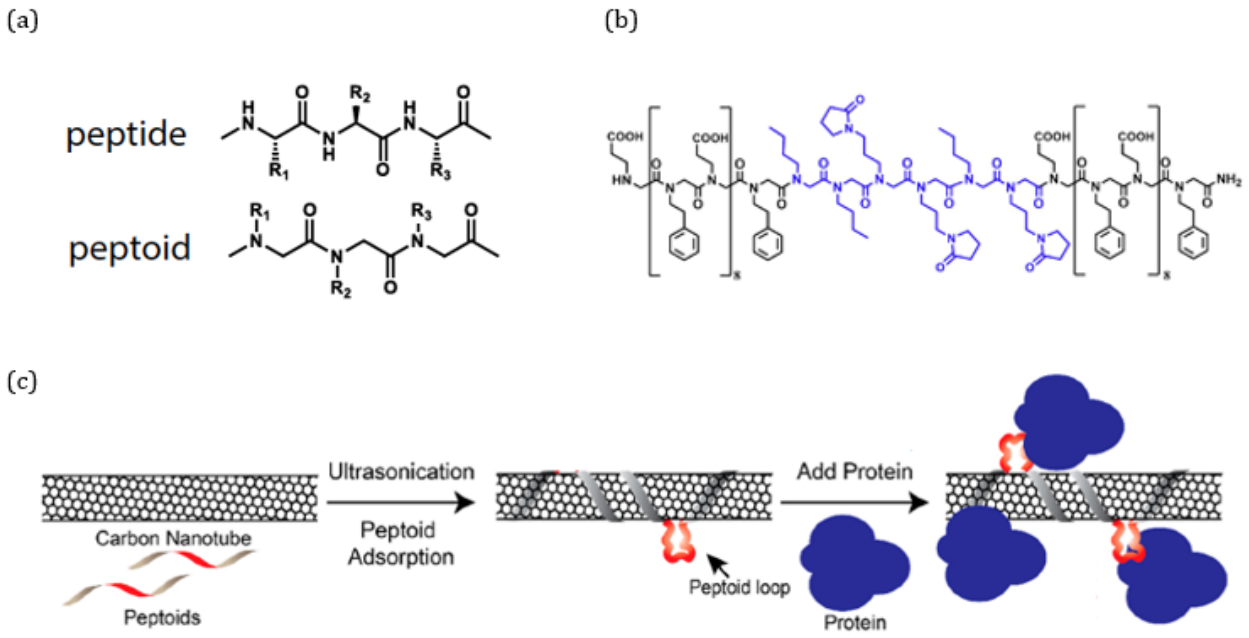

Figure 10: Peptoid-wrapped SWNTs for noncovalent protein adsorption. (a) Comparison of chemical structures for peptides (polyamino acids) and peptoids (poly-N-substituted glycines). **(b)** Example structure of a peptoid designed to bind proteins to SWNTs. SWNT-binding anchor region shown in black. Solvent-accessible protein-binding loop shown in blue. **(c)** Description of peptoid-SWNT preparation and structural schematic of peptoid-mediated protein adsorption to the SWNT surface. (a), (b), (c) adapted with permission from Chio et al, Nano Lett. 2019, 19, 11, 7563–7572. Copyright 2019, American Chemical Society.

Dually functional peptoids for SWNT conjugation and protein recognition are defined as block copolymers with two domains: an anchor region flanking a loop region (Figure 10). The anchor sequence is composed of alternating phenyl and carboxy sidechains, wherein the hydrophobic aromatic residues bind to the SWNT surface via π- π stacking interactions and anionic carboxylic acid residues impart the intramolecular repulsive forces needed for colloidal stability. Previous work shows that 8 repeats of alternating phenyl and carboxylic acid sidechains in the anchor region is optimal for suspending SWNTs[56]. The loop region is responsible for protein binding, is variable depending on the protein target, and is preferably polar to promote effective display of the recognition motif in aqueous solvent. Thus, selecting an appropriate loop sequence was the primary challenge in designing a novel peptoid-SWNT conjugate for Cas9 recognition and cellular delivery. As Cas9 is known to interact through electrostatic binding with charged ligands, we first sought to design a charged peptoid loop to bind Cas9 RNP to the SWNT surface. Cationic and anionic residues were incorporated into the peptoid loop via ethylamine and ethyl carboxy sidechains, respectively. A zwitterionic variant was also synthesized through alternating between ethylamine and ethyl carboxy sidechain additions. For increased loop solubility, thus promoting Cas9 to access surface-bound ligands, ethyl methyl ether sidechains were incorporated as a weakly polar spacer

between the loop and the hydrophobic anchor domain. Sequences for all peptoids synthesized in this study are shown in Figure 11b.

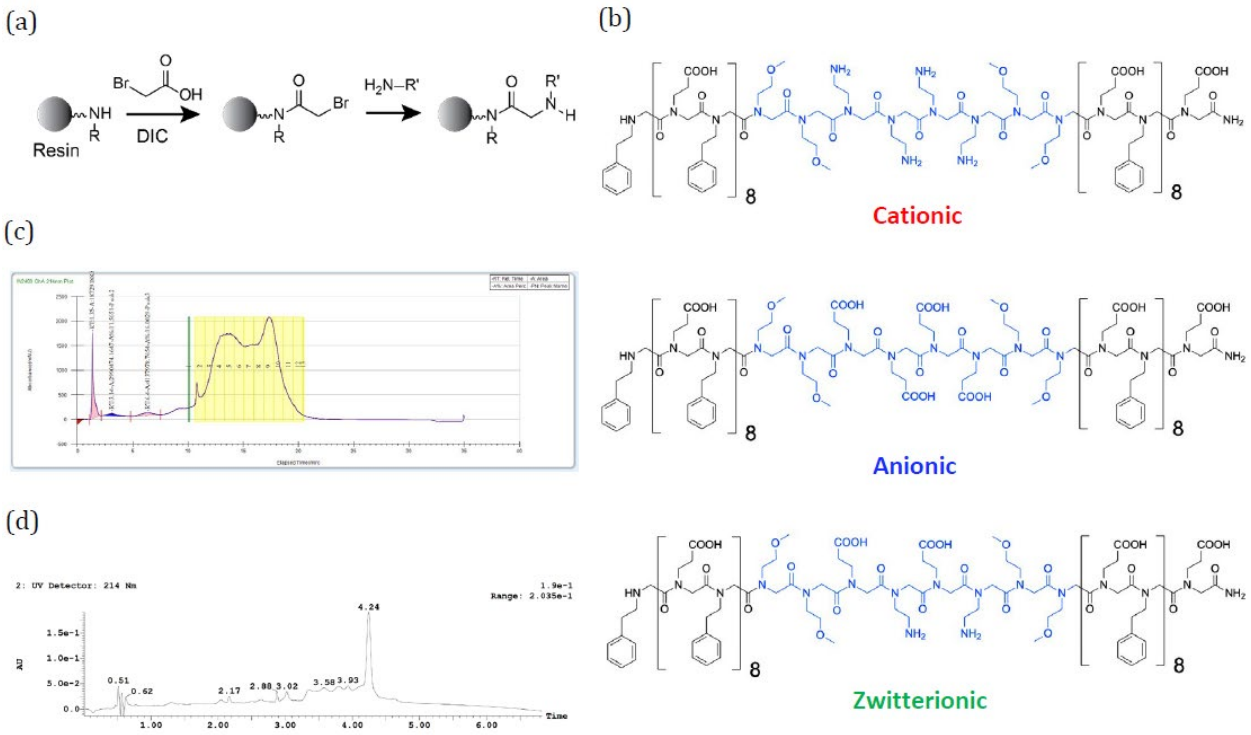

Figure 11: Peptoid-SWNT conjugates for protein delivery. (a) Solid-phase peptoid synthesis scheme by the submonomer method. Adapted with permission from Chio et al, Nano Lett. 2019, 19, 11, 7563– 7572. Copyright 2019, American Chemical Society. **(b)** Block copolymer peptoid library for electrostatic binding of Cas9 RNP. SWNT-binding anchor region shown in black. Protein-binding loop shown in blue. Representative preparative HPLC **(c)** and analytical UPLC **(d)** traces of synthetic peptoids. In (c), highlighted regions indicate the collected fractions which are then pooled and run through UPLC as shown in (d).

10.2 Peptoid Synthesis and SWNT Conjugation

Sequence-defined peptoid polymers were created by the solid-phase two-step submonomer method[57] using an automated synthesizer (Molecular Foundry, Lawrence Berkeley National Laboratory) that provides ease of synthesis especially for larger polymers with many residues (20-40). Peptoid chains are synthesized by sequential monomer addition onto Rink amide resin containing a high density of reactive amides for peptoid chain initiation (Figure 11). An amide group is activated through acylation with bromoacetic acid and the coupling agent *N,N*'-diisopropylcarbodiimide, followed by nucleophilic displacement of bromine by a primary amine bound to an R group. This two-step process is repeated with primary amines containing variable R groups that define the sequence of the peptoid polymer. To maintain chemical selectivity towards the desired product, primary amines with R groups containing nucleophilic functional groups (e.g. alcohols, carboxylic acids, off-target primary amines) were incorporated with bulky protecting groups, such as tert-

butyloxycarbonyl, appended where necessary. The automated synthesis workflow involved preparation of submonomer amines as a 1 M solution in dimethylformamide (DMF), preparation of BAA and DIC coupling agents as a 0.8 M solution in DMF, loading resin and reagent vessels onto the robotic synthesizer, and programming the instrument to perform monomer additions according to a user-defined peptoid sequence.

Once robotic synthesis was complete, resin containing surface-bound peptoid products was collected in a glass scintillation vial. A typical synthesis utilized 100 mg of resin. Acid cleavage of peptoids from resin was achieved through treatment with a cleavage cocktail containing 1.9 mL trifluoroacetic acid, 50 uL water, and 50 uL triisopropyl silane included as a cation scavenger. Cleavage proceeded for 1-1.5 hours and completion was roughly monitored by a color transformation from red to yellow. Resin was filtered out through a 2 um polypropylene frit cartridge and the TFA cleavage cocktail was evaporated to render the crude peptoid product, which typically presented as a thick orange-yellow oil. The crude peptoid was then weighed (typical crude yield ~50 mg) and dissolved in 50% acetonitrile/water for purification. Preparative HPLC was employed using a reverse-phase C18 stationary phase and an acetonitrile/water mobile phase with 0.1% TFA. Product peak separation, as measured by absorbance at 214nm, was suboptimal due to the high number of nonpolar residues present in SWNT-binding peptoids, but fractions collected from the far end of the broad overlap between dominant elution peaks (RT ~ 15-20 minutes) were of high purity (Figure 11c). Product purity and confirmation of the expected molecular weight were verified by UPLC/MS of HPLC fractions, and the 3-4 purest fractions were then pooled and lyophilized to use for SWNT conjugation. Pure lyophilized peptoid product typically presented as a thin white film.

To prepare noncovalent peptoid-SWNT conjugates, pure lyophilized peptoid was dissolved in DMSO at a known concentration (1-5 mg/mL). SWNTs produced by high-pressure carbon monoxide (HiPCO) catalytic synthesis were obtained as a raw hydrated paste containing a mixture of 10 wt% SWNT bundles along with water, amorphous carbon, and residual iron catalyst. This cake was distributed into a slurry containing roughly 2 mg/mL SWNT in water for easier handling. 100 uL of peptoids in 100% DMSO was then combined with SWNT at a 2:1 mass ratio of peptoid:SWNT in 1 mL final volume of 50 mM borate buffer, pH 9. The mixture was bath sonicated for 10 minutes followed by pulsed (1 second on/1 second off) probe tip ultrasonication on ice for 10 minutes net sonication time. Successful SWNT suspension, as evidenced by a dark gray/black homogenous liquid, was first verified by visual inspection of the sample after sonication. Crude suspensions were allowed to equilibrate for 30 minutes at room temperature. Unsuspended starting material and residual impurities were then pelleted by centrifugation at 17,000 xg for 90 minutes and the supernatant, containing only free unbound peptoid and individually suspended peptoid-SWNTs, was collected. Free peptoid was removed through successive filtration steps involving spin filtration through a 100K MWCO cellulosic membrane followed by redilution in 50 mM borate, pH 9. Centrifugation speed and duration were optimized such that each filtration step accomplished a ~5x dilution of free peptoid without excessively concentrating the suspension to the point of slurry formation. Spin filtration was considered complete when free peptoid could no longer be detected in the flowthrough, as measured by absorbance at 214 nm (typically 7-10 filtration cycles). SWNT concentration in the purified

suspension was measured by absorbance at 632 nm (ε = 0.036 L mg^{-1} cm^{-1}), and typically yielded 30-70 mg/L SWNT in 500 uL from ~50-100 ug raw SWNT input.

10.3 Cas9 Ribonucleoprotein Assembly and *In Vitro* Cleavage Assay

Wildtype Cas9 from *Streptococcus pyogenes* fused to an SV40 nuclear localization sequence (spCas9-NLS, 161 kDa) was obtained as a recombinant protein purified from *E. coli* (Macrolab, UC Berkeley) in frozen aliquots containing 40 uM Cas9 in 20 mM HEPES-KOH pH 7.5, 150 mM KCl, 10% glycerol, 1 mM DTT. In its apo form (i.e. without sgRNA), Cas9 is known to be sensitive under *in vitro* handling conditions and may become irreversibly inactivated even under moderate thermal stress. All protein stocks were stored at -80 C and care was taken to not expose stocks to multiple freeze/thaw cycles. Prior to assembly with sgRNA, Cas9 stocks were thawed on ice and exposure to elevated temperatures, which could inhibit RNP formation, was strictly limited. sgRNA was purchased as a synthetic oligonucleotide containing 2'-Omethyl and 3' phosphorothioate chemical protecting groups and a proprietary scaffold along with the user-specified spacer sequence. Chemically protected sgRNA has been shown to improve gene editing proficiency due to resistance against endogenous RNAses and prolonged cellular half-life[58]. In addition, RNase-resistant sgRNA is simpler to handle in a lab setting where environmental RNAse contamination is a common risk. All sgRNA reagents were stored at -20 C as 10 uM stocks in 10 mM Tris pH 8, 1 mM EDTA and kept on ice during assay preparation.

Cas9-sgRNA ribonucleoprotein assemblies were prepared by coincubation of Cas9 and sgRNA at a 1.5:1 molar ratio of Cas9:sgRNA in a suitable assembly buffer. 40 uM Cas9 stocks were often first diluted in assembly buffer to a working concentration of 1-5 uM before assembly. To form RNPs, sgRNA stocks were first diluted in assembly buffer and well-mixed. To minimize local aggregation during protein dilution, Cas9 was then diluted slowly, and with gentle intermittent mixing, into the sgRNA solution and incubated at 37 C for 5 minutes. Assembled RNPs were then kept on ice until use. Several buffers were used to assay colloidal and enzymatic behavior of Cas9 RNP under conditions relevant to SWNT-mediated plant cellular delivery. Routinely, RNP assembly was done in 20 mM HEPES pH 7.4, 150 mM NaCl due it's maximal compatibility with optimal buffer conditions for SWNT. In general, Cas9 is most stable near neutral pH in buffers with an ionic strength at or above cellular (150-200 mM) to prevent aggregation. Added Mg^{2+} may improve activity especially for *in vitro* screening as the Cas9 nuclease domains RuvC and HNH are known to be magnesium dependent.

Cas9 enzymatic activity was screened *in vitro* via a cleavage assay on dsDNA substrate containing the target sequence for sgRNA-mediated endonuclease activity. dsDNA substrate was generated by PCR as an 800 bp amplicon from plant genomic DNA and gene-specific primers for PDS or GFP target loci. 150 ng dsDNA substrate was combined with preassembled Cas9 RNP in 20 mM HEPES pH 7.4, 150 mM NaCl at a 10:1 molar excess of RNP:DNA. Cleavage was allowed to proceed for 16 hrs at 37 C followed by heat inactivation for 10 mins at 65 C to unbind Cas9 from the substrate. As cleavage products separate well from uncleaved substrate by agarose gel electrophoresis, the emergence of two cleavage

bands at lengths predicted by the Cas9 cut site and the corresponding signal reduction in the longer uncleaved substrate band is a clear and reliably quantifiable indication of Cas9 activity *in vitro*. After heat inactivation, 2.5 uL of the reaction mixture was then separated by agarose gel electrophoresis and image analysis was used to quantify Cas9 activity by the percent of cleaved substrate relative to total band signal.

10.4 Enzymatic Activity of Cas9 RNP-peptoid-SWNTs

As discussed previously, SWNTs may deactivate Cas9 targeted cleavage functionality through nonspecific interactions or due to the high charge density of electrostatically functionalized SWNTs. Thus, we sought to investigate the enzymatic activity of Cas9 when complexed to peptoid-SWNTs using an *in vitro* cleavage assay, as depicted in Figure 12a. Upon coincubation with a dsDNA substrate containing the target sequence specified by the sgRNA, Cas9 is directed to the target sequence and performs a double-stranded break, resulting the formation of two dsDNA products with predictable lengths designated by the location of the cut site and the total size of the uncleaved dsDNA substrate. The reaction mixture is then separated and visualized by agarose gel electrophoresis, wherein the uncleaved band will appear at a high molecular weight than the two cleaved bands (Figure 10b). Cas9 activity is then quantified through image analysis by integrating the band intensities and calculating activity according to the following equation: % activity = 100* $\sum$(cleaved) / $\sum$(cleaved and uncleaved). Results for Cas9 activity at increasing concentrations of peptoid-SWNTs and variable loop identities are summarized in Figure 12c. The peptoid loop identity was found to have negligible effect on Cas9 activity, as evidenced by nearly identical trends across cationic, anionic, and zwitterionic peptoid loops. However, peptoid-SWNT concentration was shown to have the strongest effect on Cas9 activity. While 0.1 mg/L and 1 mg/L peptoid-SWNT showed no cleavage inhibition compared to the control not containing SWNT, 5 mg/L peptoid-SWNT caused approximately 50% reduction in activity regardless of loop identity. Higher concentrations of SWNT, up to 50 mg/L, were shown to further inhibit Cas9 cleavage up to 90%. For downstream applications, peptoid-SWNT concentrations were kept below the acceptable inhibition threshold of 5 mg/L in order to maintain Cas9 structural integrity and enzymatic function.

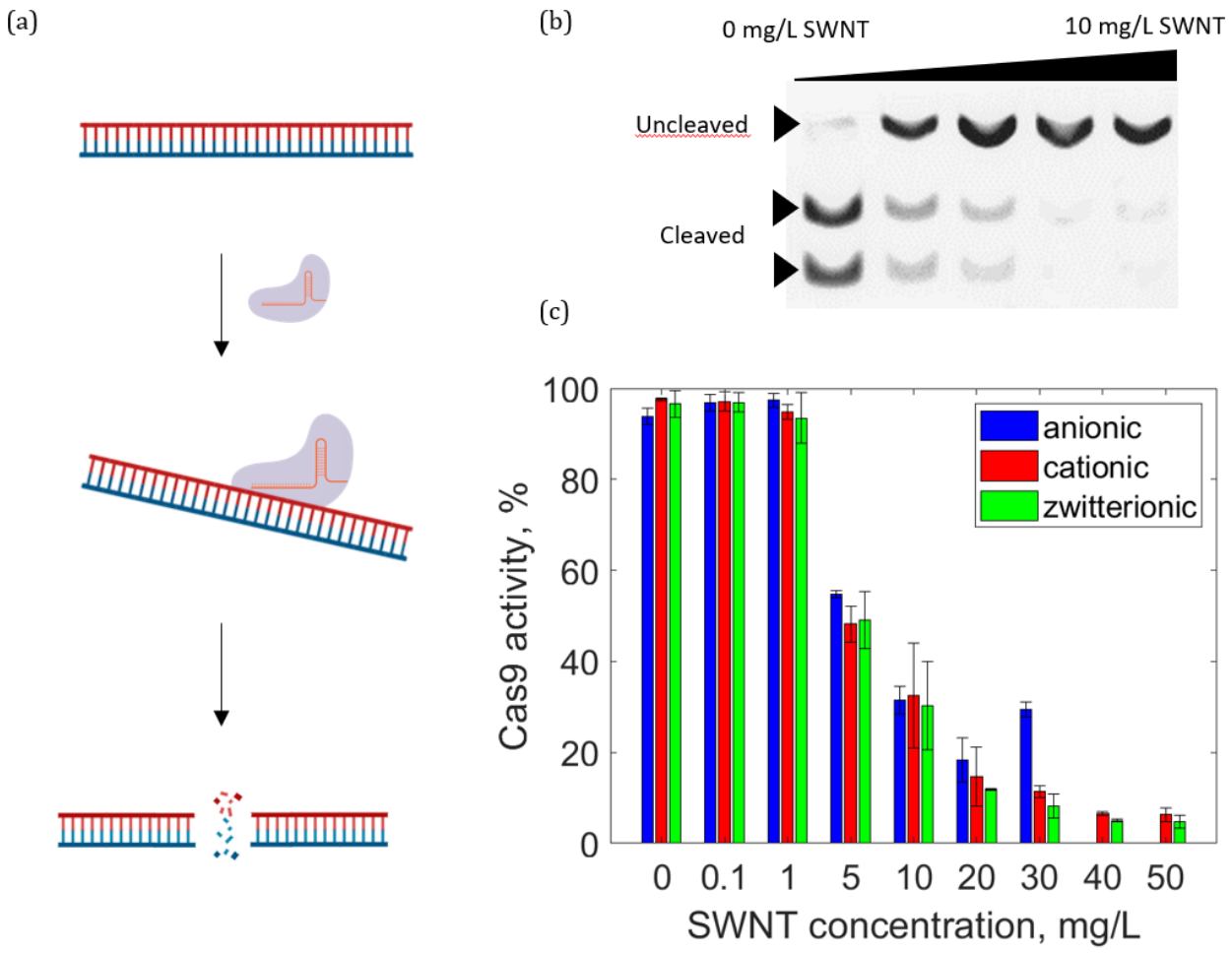

Figure 12: Cas9 RNP enzymatic activity upon peptoid-SWNT complexation. (a) Schematic of the *in vitro* cleavage assay used to measure Cas9 RNP enzymatic activity. Double-stranded DNA (orange/blue) containing the sgRNA target sequence is bound by Cas9 RNP (purple/orange) and cleaved to generate two dsDNA products. **(b)** Representative data for agarose gel electrophoresis of purified DNA cleavage products obtained from reactions containing increasing amounts of peptoid-SWNT. Low molecular weight cleaved bands represent successful Cas9 enzymatic activity, while high molecular weight uncleaved bands indicate reduced enzymatic activity. **(c)** Comparison of Cas9 enzymatic activity when complexed to variable concentrations and loop structures of peptoid-SWNTs. Cas9 activity is calculated using integrated band intensity from an agarose gel, i.e. % activity = 100* ∑(cleaved) / ∑(cleaved and uncleaved).

10.5 Dynamic Light Scattering of Protein-SWNT Complexes

RNPs were preassembled in 20 mM HEPES pH 7.4, 150 mM NaCl at a working concentration of 0.25 uM. Peptoid-SWNTs were diluted to 20 mg/L working concentration in 20 mM HEPES, 150 mM NaCl and bath sonicated for 10 minutes after dilution. Directly

prior to measurement, peptoid-SWNTs and Cas9 RNP were combined in buffer at a defined molar ratio of protein:SWNT to a final SWNT concentration of 5 mg/L in 40 uL total volume. The entire sample was transferred to a clean Malvern ZEN0040 microcuvette for analysis, taking care to avoid bubble formation. Cuvettes were reused for 20-30 samples and rinsed thoroughly 3x with water followed by 70% ethanol using a vacuum-equipped cuvette washer. Dynamic Light Scattering (DLS) measurements were taken on a Malvern Zetasizer NanoZS in backscattering mode (173^{o} detector angle) and raw scattering data were correlated by the non-negative least squares (NNLS) algorithm. For comparison, CONTIN regularization was also applied, under the pretense that the chosen correlation algorithm could have a large effect on results due to the colloidal complexity of RNP-peptoid-SWNTs, but CONTIN was found to produce similar results to NNLS (data not shown).

10.6 Colloidal Stability of Cas9 RNP-peptoid-SWNTs

Protein-SWNT conjugate colloidal stability is important to maintain individually suspended nanoparticles and prevent protein aggregation, which has dual importance both in preserving enzymatic activity and keeping the carrier particle size below the size exclusion limit of the cell wall. Dynamic light scattering (DLS) is a common technique used to measure nanoscale particle radii through analysis of scattered light incident on a nanoparticle sample (Figure 14a). Correlation of scattering profiles taken at discrete temporal intervals allows one to calculate the particle diffusivity and subsequently, through the Stokes-Einstein equation, particle radius. However, as the Stokes-Einstein equation is valid only for spherical particles, the particle radius as measured by DLS has little meaning high-aspect ratio cylindrical nanoparticles such as SWNTs. Size distributions of SWNTs measured by DLS are often bimodal and difficult to interpret (Figure 14a), which limits the application of traditional workflows for measuring particle size using this technique. Therefore, we focused instead on the particle diffusivity as a straightforward metric for measuring colloidal stability of RNP-peptoid-SWNT conjugates. In particular, we analyzed the change in particle diffusivity as a function of peptoid loop identity and increasing molar ratios of Cas9 RNP:SWNT. Absent of intramolecular interactions, particle size is directly correlated to diffusivity, wherein larger particles exhibit reduced Brownian motion and, therefore, have lower diffusivity. Repulsive and attractive interactions between particles can result in positive and negative changes to diffusivity, respectively, due to aggregate formation or the effects that intramolecular forces have on Brownian motion of suspended particles. As Cas9 RNP holds a bulk negative charge and is large in comparison to SWNT particle size, introducing increasing amounts of protein to peptoid-SWNTs results in competing effects on particle diffusivity due to increased particle size (Cas9 adsorption) and increased bulk charge density (intramolecular repulsion).

The effects of particle size and intramolecular repulsion on RNP-peptoid-SWNT diffusivity as measured by DLS are shown in Figure 14c and Figure 14d. Peptoid loops containing cationic charged groups result in optimal stability of RNP-peptoid-SWNTs up to a protein:SWNT molar ratio of 10:1. Peptoid-SWNTs containing purely cationic loops

maintained enhanced stability at lower ratios (1:1 to 5:1) compared to zwitterionic loops, further emphasizing the role of cationic ligands in RNP-SWNT conjugate stabilization. In

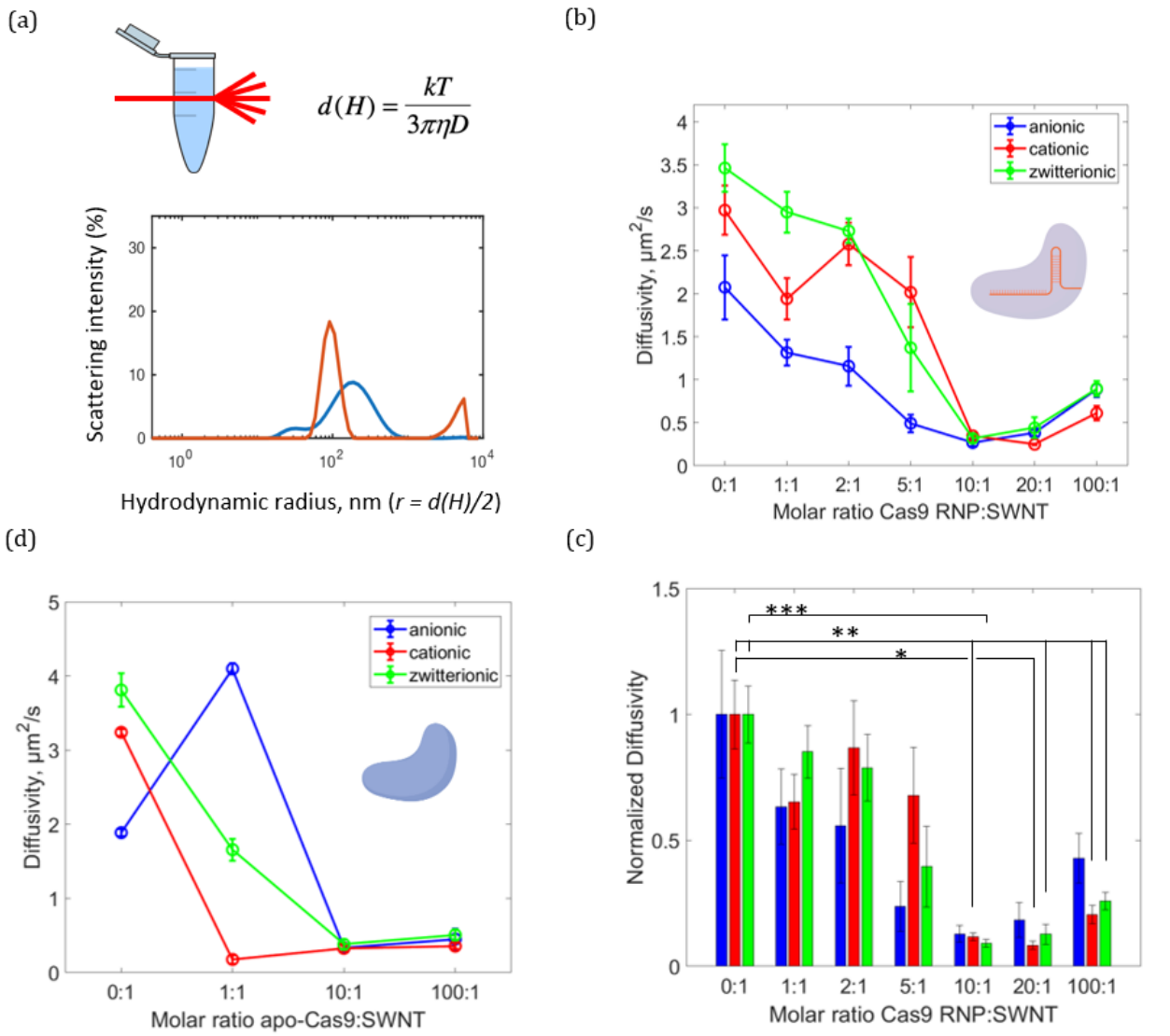

Figure 14: Dynamic light scattering to measure colloidal stability of RNP-peptoid-SWNTs. (a) Schematic of light scattering by colloidal particles. Scatter signal is temporally correlated to yield the average particle diffusivity, D, which is then used to calculate the equivalent spherical particle hydrodynamic diameter, d(H), using the Stokes-Einstein equation. An example intensity distribution of peptoid-SWNTs is given to demonstrate that the Stokes-Einstein equation to fails to yield interpretable results for cylindrical SWNT particles. **(b)** Diffusivity of RNP-peptoid-SWNTs as measured by DLS at varying molar ratios of Cas9 RNP:SWNT and variable peptoid loop identities. **(c)** Diffusivity of RNP-peptoid SWNTs normalized to a 0:1 molar ratio of RNP:SWNT (i.e. SWNT only, no protein). Bar colors correspond to the legend in (b). Asterisks indicate statistical significance from Tukey's t-test (*** = $p < 0.001$, ** = $p < 0.01$, * = $p < 0.05$, no asterisk = ns). **(d)** Diffusivity of apo-Cas9-

peptoid-SWNTs as measured by DLS at varying molar ratios of Cas9 RNP:SWNT and variable peptoid loop identities. apo-Cas9 = Cas9 with no sgRNA.

contrast, peptoid-SWNTs containing the anionic peptoid loop were significantly destabilized upon protein addition even at lower protein:SWNT ratios (5:1). However, this trend was found to be opposite when apo-Cas9 (i.e. without sgRNA) was conjugated to peptoid-SWNTs, presumably due to the differing charge between apo-Cas9 (overall positive) and Cas9 RNP (overall negative). Peptoid-SWNTs containing purely anionic groups were shown to stabilize apo-Cas9 up to a molar ratio of 10:1, whereas peptoid-SWNTs containing cationic groups were highly destabilized by apo-Cas9 even at a 1:1 molar ratio. In addition, we considered the effect that free protein might have on the measured diffusivity due to the sensitivity of the DLS measurement to convolution between scattering from SWNT and protein species present in suspension. However, free protein diffusivity was not found to be concentration-dependent within the range investigated (Figure 15). In other words, the free protein detection limit was far below what was used in all studies involving peptoid-SWNTs, therefore eliminating any measurable contribution from free protein when analyzing RNP-peptoid-SWNT conjugates. Taken together, we conclude from these DLS studies that cationic peptoid ligands are optimal for a stable RNP-peptoid-SWNT colloid to be used for plant cellular delivery.

(a)

molar excess RNP	*SWNT (mg/mL)*	*SWNT (uM)*	*RNP (uM)*
0	10	0.003	0
1	10	0.003	0.003
10	10	0.003	0.03
100	10	0.003	0.3
0	5	0.0015	0
1	5	0.0015	0.0015
10	5	0.0015	0.015
100	5	0.0015	0.15
0	1	0.0003	0
1	1	0.0003	0.0003
10	1	0.0003	0.003
100	1	0.0003	0.03

(b)

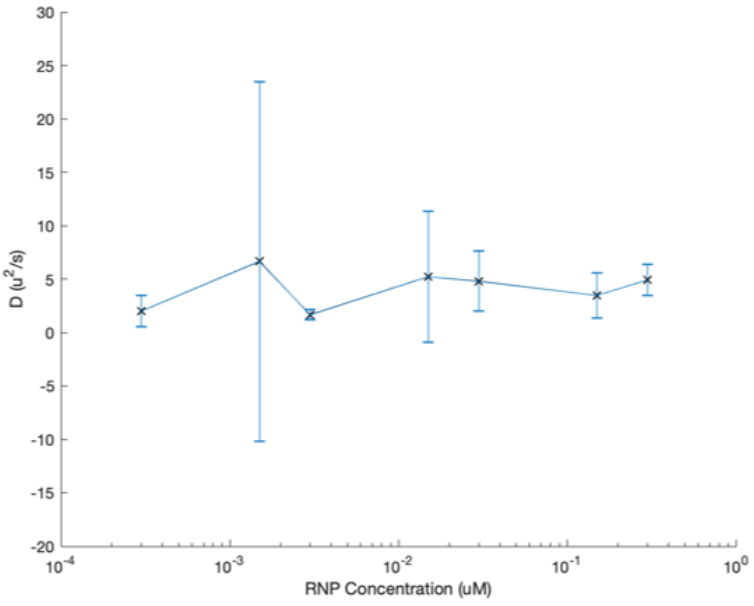

Figure 15: Sensitivity of DLS measurements to free protein. (a) Table showing working concentration of RNP at varying SWNT concentrations and molar ratios of RNP:SWNT used in the DLS studies shown in Figure 14. **(b)** Particle diffusivity of RNP across the range of working concentrations shown in (a).

10.7 Atomic Force Microscopy of Protein-SWNT Complexes

Functionalized APS-mica substrates were prepared as described previously[59]. Aminopropyl silatrane (APS) was synthesized through an NaOH-catalyzed condensation reaction between triethanolamine and (3-aminopropyl)triethoxysilane (APTES). Precise stoichiometric amounts of triethanolamine (14.92 g) and APTES (22.14 g) were combined in 10 mL methanol containing 2 mg/mL NaOH. The reaction mixture was placed on a rotary evaporator at 40 C under mild vacuum (100 torr) until all the methanol evaporated. The temperature was then raised to 60 C and pressure lowered gradually to 1 torr, allowing for ethanol produced during the reaction to continuously evaporate off. After 1.5 hours, the reaction mixture was removed from heat and vacuum and cooled on ice to initiate product crystallization. The solid product was then redissolved in 15 mL warm methanol and 150 mL toluene. The mixture was partially evaporated to approximately half of the volume and recrystallized overnight at 4 C. The recrystallized solid was gently agitated to break up large crystals and then collected by vacuum filtration through a glass filter followed by 2x wash with 20 mL ice-cold toluene before brief drying under vacuum. 8.4 g of solid APS product was collected and stored under inert gas with desiccant at 4 C. To generate APS-functionalized mica surfaces, freshly cleaved mica was soaked in 166 nM APS in water for 30 minutes at room temperature to allow covalent attachment of cationic APS to the negatively charged mica surface. The functionalized APS-mica sheets were then gently rinsed 3x with water and stored under N2 with desiccant at 4 C until use. Care was taken not to touch the mica surface after cleavage and functionalization.

AFM sample preparation of RNP-peptoid SWNTs was first done by coincubation of preassembled RNP and peptoid-SWNTs at 10 mg/L SWNT and a defined molar ratio of Cas9:SWNT. 20-30 uL of RNP-peptoid-SWNTs was then spread across the surface of an APS-mica chip affixed to a magnetic AFM sample disk and allowed to sit at room temperature for 10 minutes to allow surface adsorption. The APS-mica surface was then rinsed liberally with DI water and gently blown dry with nitrogen. Sample chips were prepared directly prior to imaging with TAP150AL-G aluminum-coated AFM probes (<8 nm tip radius) on an Asylum MFP-3D operating in tapping mode. Fresh probes were used for each sample or upon tip malfunction/breakage; on average two images of the same sample were collected per probe. All images were taken using identical scan rates and pixel numbers to maintain consistent tip behavior and resolution across samples. Generation of a cationic APS-mica surface for imaging RNP-peptoid-SWNTs was found to greatly improve image quality through improved sample deposition and uniformity, as well as reducing static charge buildups that complicate AFM operation and interfere with AFM data quality.

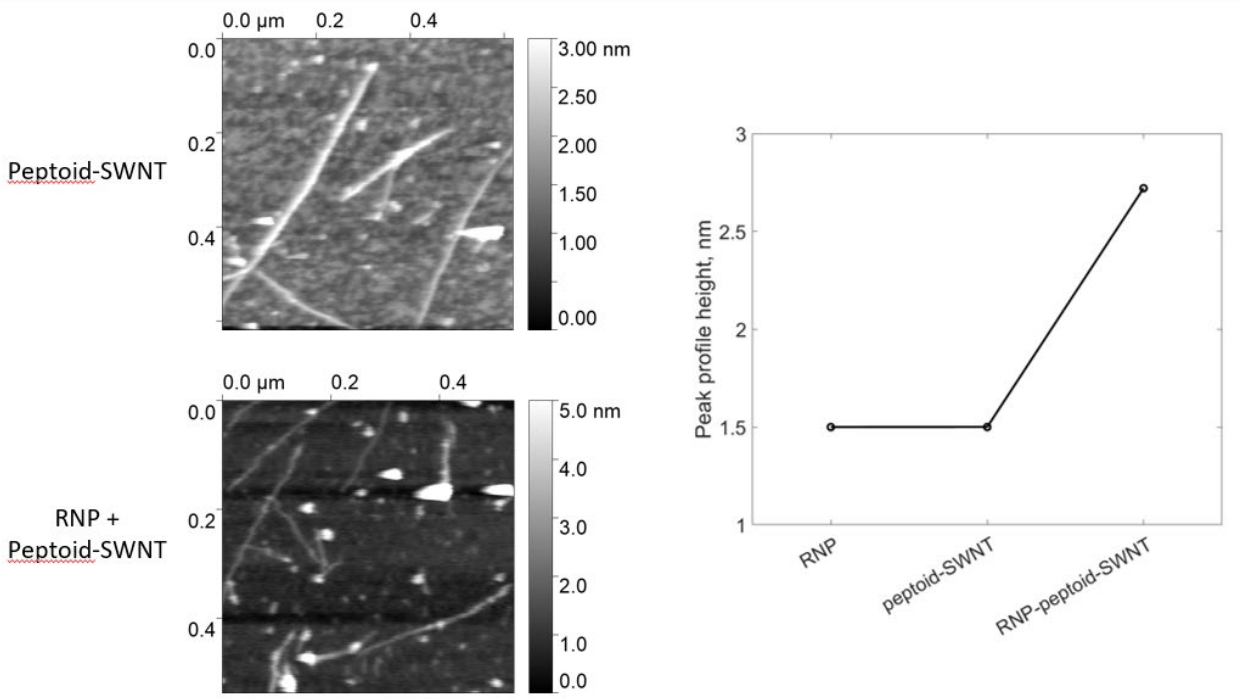

Figure 13: Atomic Force Microscopy of RNP-peptoid-SWNTs. (a) Representative AFM images of peptoid-SWNTs (top) without protein and complexed RNP-peptoid-SWNTs (bottom). **(b)** Average peak AFM profile height of RNP, peptoid-SWNT, and RNP-peptoid-SWNTs. The sum of RNP and peptoid-SWNT approximately equals the peak profile height of RNP-peptoid-SWNTs, indicating successful surface conjugation of RNPs to peptoid-SWNTs.

10.8 Visualizing Protein Binding by Atomic Force Microscopy

Direct visualization of Cas9 RNP bound to the peptoid-SWNT surface is possible through Atomic Force Microscopy (AFM). A representative AFM image of RNP-bound peptoid-SWNTs containing a cationic ligand loop is shown in Figure 13a. When imaged absent of RNP, peptoid-SWNTs appear as fiber-like particles several 100 nm in length and 2-3 nm in diameter. At this resolution, the peptoid-SWNT height profile is constant along the length of the nanotube, as individual peptoid binding sites on the SWNT surface are not resolved in these images. Upon complexation with preassembled RNPs, individual RNPs (1.5-2 nm) are visible decorating the SWNT surface along with free unbound RNP adsorbed to the mica imaging surface. We note that RNP diameter on a dehydrated mica surface is expected to be much smaller than the diameter of hydrated RNP in solution (~2 nm on AFM vs ~10 nm by DLS). Through image analysis software, linear height profiles were extracted for free unbound RNP as well as along the length of peptoid-SWNTs and RNP-peptoid SWNTs. The peak profile height is reported in Figure 13b. Free RNP and peptoid-SWNTs both average ~1.5 nm in height as measured by AFM. Upon complexation to RNPs, peptoid-SWNT peak profile height increases to 2.7 nm, approximately the sum of peak profile heights for

RNP and peptoid-SWNTs individually, suggesting that surface-bound features are attributable to RNP adsorption.

10.9 Peptoid-SWNT Mediated Delivery of Active RNPs to Leaves

To assay successful peptoid-SWNT mediated delivery to leaves and subsequent CRISPR-induced mutations, we chose the model gene target *phytoene desaturase* (PDS) in *Nicotiana benthamiana*. The PDS gene product is involved in carotenoid biosynthesis and is commonly used as a model gene target in plants due to the visible phenotype (white leaves) upon successful gene knockout. Based on results from the DLS studies, we hypothesized that colloidal stability would play a role in delivery efficiency. To that end, we delivered RNP-peptoid-SWNT conjugates at variable ratios of protein:SWNT for peptoid loops containing charged ligands via leaf infiltration to mature *N. benthamiana* leaves and measured indel frequency via TIDE. The detection threshold for these experiments was determined to be 2% based on TIDE analysis of a buffer-infiltrated control. In line with the DLS studies, peptoid loops containing cationic ligands performed the highest overall with respect to mutation frequency, however some unexpected trends did emerge. RNPs delivered using the

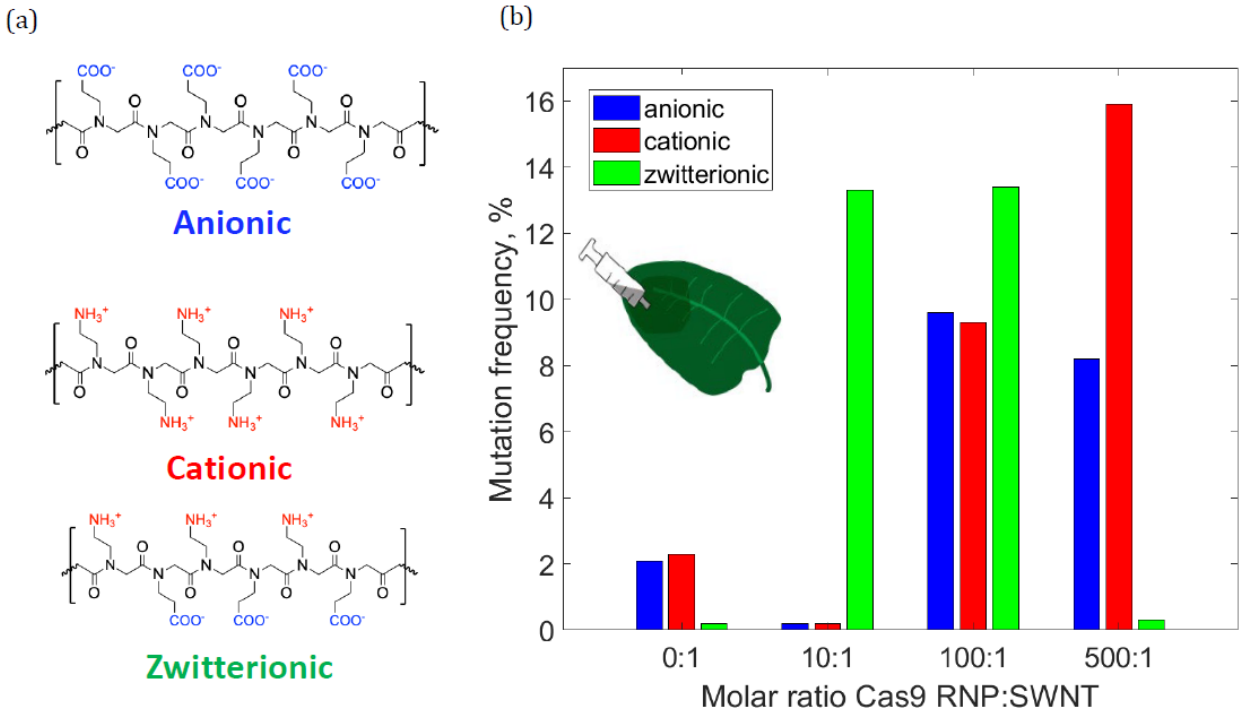

Figure 16: Peptoid-SWNT mediated RNP delivery in leaves. (a) Peptoid-SWNT loops for electrostatic binding to SWNTs. **(b)** Mutation frequency as measured by TIDE for *Nicotiana benthamiana* leaves infiltrated with RNP-peptoid-SWNTs at variable ratios of RNP:SWNT (N=1). Gene target is phytoene desaturase, specified by NbPDS sgRNA.

zwitterionic peptoid loop showed the highest mutation frequency for 10:1 and 100:1 ratio of approximately 13%, but did not induce any mutations at a 500:1 protein:SWNT ratio. In contrast, the cationic and anionic peptoid loops did not induce any mutations at a 10:1 molar ratio, but did induce mutations at 100:1 and 500:1, with the cationic peptoid resulting in the highest overall mutation frequency of 16% across all conditions studied in this experiment. This suggests that there are additional factors affecting delivery efficiency and mutation frequency apart from *in vitro* colloidal stability alone. We note that total RNP dosage could be a factor, as higher molar ratios of protein:SWNT contain a greater amount of protein infiltrated into the leaf. However, dose response alone is not sufficient to explain all of the observed trends, as the zwitterionic peptoid performed nearly identically at a 10:1 and 100:1 ratio, but resulted in no measurable mutations at the highest dosage of 500:1. Therefore, we suggest that the introduction of RNP-peptoid-SWNTs to the complex biological environment inside of a leaf has the strongest influence on mutation frequency such that predicting a successful conjugate *in vitro* is challenging and colloidal characterization alone is insufficient.

11. sgRNA-SWNTs for cellular delivery of RNA

Nucleic acid-wrapped single-walled carbon nanotubes (SWNTs) have distinct optical and physical properties leading to their use in many biological applications including biomolecule delivery and fluorescence-based sensing. While most applications utilize DNA-SWNT conjugates in a mammalian biological context, our lab has demonstrated the utility of RNA-SWNTs as a gene-silencing tool in plant leaves via the delivery of active small interfering RNA (siRNA) noncovalently attached to pristine SWNTs.[60] In this previous work, SWNTs were shown to protect siRNA against degradation by endoribonucleases as well as improve cellular uptake of siRNA into the plant cell, thus improving silencing efficiency compared to free siRNA alone. In our present work, we seek to expand the application of RNA-SWNTs in plant cells to include RNA with cellular functions beyond gene silencing, namely the class of RNA molecules that are used in programming targets for CRISPR gene editing (tracrRNA + crRNA or sgRNA). We hypothesize that delivering SWNTs to transgenic plant cells constitutively expressing Cas9 could lead to and improve gene editing efficiency through increased cellular uptake and protection of guide RNAs against degradation. We propose that such a platform could be used to improve the throughput of gene target screening, which could have a significant potential impact on gene editing workflows given that guide RNA design is known to significantly affect gene editing outcomes but these effects are difficult to predict based on guide RNA sequence alone. Furthermore, we envision that these RNA-SWNTs could in the future be applied alongside a Cas9 protein delivery strategy to accomplish DNA-free gene editing outcomes without transgenic plants, both in model plant species used in fundamental research as well as crop cultivars relevant to agriculture.

In this work, we tested several varieties of RNA used for gene editing with Cas9: single-guide RNA (sgRNA), CRISPR RNA (crRNA), and trans-activating CRISPR RNA (tracrRNA). crRNA and tracrRNA are the dual RNA components discovered in the wildtype Cas9 system, wherein crRNA (36nt) contains the target information and tracrRNA (67nt) contains the structural motif necessary for binding crRNA to Cas9. sgRNA (100 nt) is a synthetic chimera of the crRNA and tracrRNA and contains both the target sequence and the

structural motif required to bind Cas9. RNA is purchased commercially as a synthetic oligonucleotide with chemical modifications to protect against environmental exoribonucleases, which greatly simplifies handling and storage.

11.1 Preparation of sgRNA-SWNTs

RNA-SWNTs are prepared as described previously for siRNA SWNT suspensions[61] and shown in Figure 17; we note that all three RNA types surveyed in this work were successful at suspending SWNT with identical preparation protocols. 50-500 ug of RNA are combined with raw SWNTs in 100 mM NaCl at a 2:1 mass ratio of RNA:SWNT and probe-tip sonicated for 30 minutes. The raw suspension is then centrifuged at high speed (15000-20000 rcf) for 60 minutes to pellet unsuspended SWNT bundles as well as amorphous carbon and residual catalyst leftover from SWNT synthesis. Approximately 40-60% of the total RNA is adsorbed onto individual SWNTs, and the remaining RNA free in solution is removed via 7-10 spin filtration steps through a 100K MWCO cellulosic membrane that allows free RNA to pass through with minimal loss of suspended SWNTs. A successful SWNT suspension is initially verified by eye, as colloidal SWNTs should appear as a homogenous gray/black liquid (Figure 17B). A stable RNA-SWNT suspension is further confirmed by near-infrared (nIR) fluorescence spectrometry (Figure 18A), wherein strong nIR emission indicates the presence of individually suspended SWNTs (as bundled SWNT aggregates are highly quenched). Furthermore, we note the stability of RNA-SWNTs over time, as indicated by no loss in nIR fluorescence emission over the course of two months when stored at 4oC (Figure 18B). sgRNA, crRNA, and tracrRNA suspend SWNTs to a high concentration (50-100 mg/L SWNT in 1 mL) and with reproducible yield similar to DNA-SWNTs; an important finding, as the cost of synthetic RNA oligonucleotides at the scale required for SWNT conjugation greatly exceeds the cost of DNA oligonucleotides of similar length. We hypothesize that either unfiltered RNA-SWNT (free RNA + adsorbed RNA) or filtered RNA-SWNT (adsorbed RNA, only) could function as an effective conjugate for delivery applications, so samples were collected before and after filtration for use in downstream assays.

11.2 Characterizing sgRNA-SWNTs for *in planta* delivery

As the types of guide RNA used in this work (36-100nts) are longer than siRNAs used previously (20-25nts), and also require folding into a secondary structure to bind Cas9, we first sought to measure if the guide RNA structural integrity is maintained after ultrasonication with SWNTs. In order to assay the functionality of sgRNA, crRNA, and tracrRNA suspended onto SWNTs, we performed Cas9 in vitro assays. In this assay SpCas9 protein is mixed with SWNT-RNA suspensions (both unfiltered and filtered), Cas9 Buffer (100 mM NaCl, 50 mM Tris-HCl, 10 mM MgCl2, 1 mM DTT, pH 7.9), PCR template DNA containing the CRISPR guide RNA target sequence, and incubated at 37oC for 8 hours. Cas9 mixed with free sgRNA or crRNA/tracrRNA were used as positive controls and Cas9 alone (no sgRNA, crRNA and tracrRNA) were used as negative controls (Figure 19). Functional

RNPs (Cas9 complexed with guide RNA) are able to cleave the template DNA (757bp) and when run on agarose gel two fragments can be observed (440 and 313bp)(Fig. 19, Lane 2),

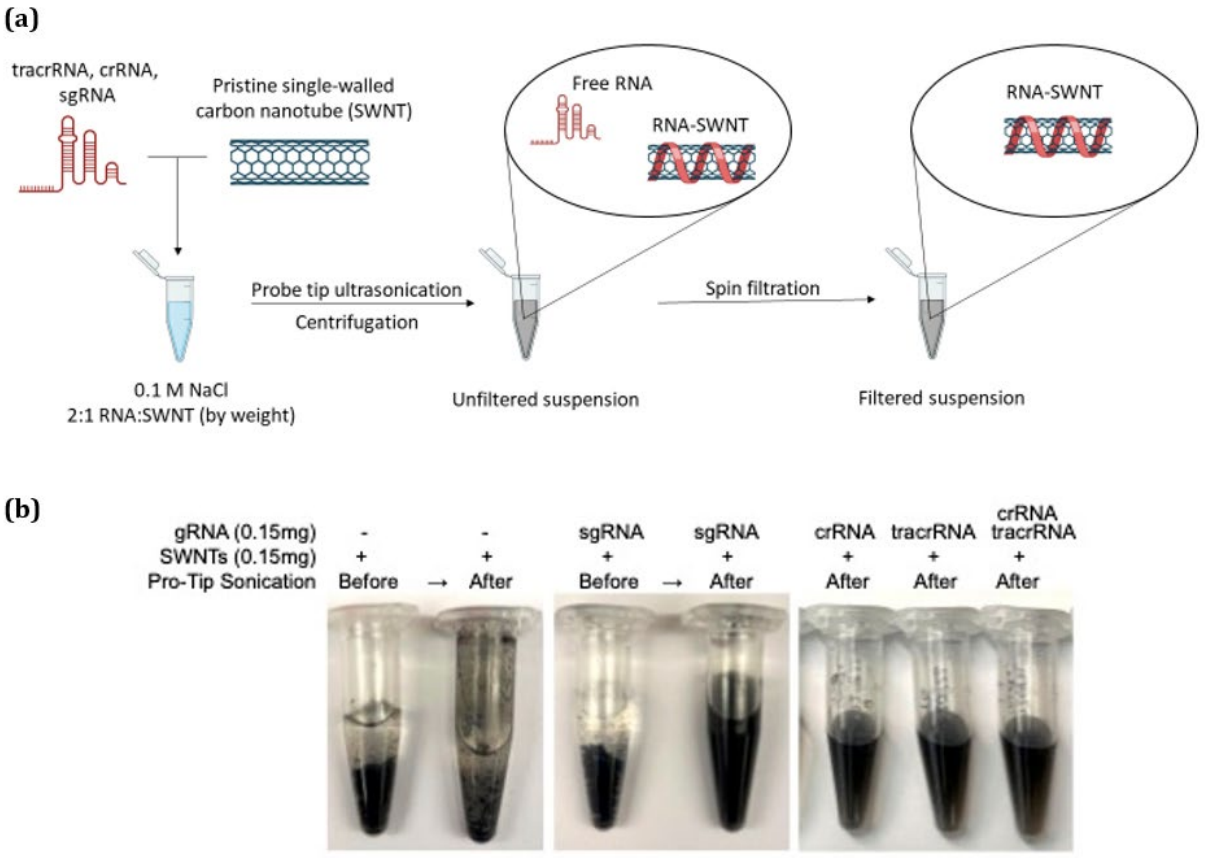

Figure 17. CRISPR RNA-SWNT preparation and colloidal stability. (a) Loading of Guide RNAs (sgRNA, crRNA and/or tracrRNA) onto SWNTs is accomplished by mixing 2:1 RNA:SWNT followed by probe-tip sonication. The resulting suspension appears homogeneous and gray/black in color, serving as a visual check for a successful noncovalent adsorption of guide RNAs onto SWNTs via π-π-stacking interactions. **(b)** Guide RNAs-SWNT suspensions are colloidally stable after probe-tip sonication. Photos of guide SWNT mixtures without RNA (Left), with sgRNA (middle), and with crRNA, tracrRNA, or an equimolar mix of crRNA/tracrRNA (Right) before and after pro-tip sonication. while uncleaved DNA template indicates an absence of RNP in vitro activity (Fig. 19A, Lane 3). When incubated with Cas9 Buffer, unfiltered SWNT-RNA suspensions led to template DNA cleavage (Fig. 19A, Lanes 4 and 6), while filtered suspensions did not (Fig. 19A, Lanes 5 and 6) suggesting that free (unbound) sgRNA or crRNA/tracrRNA in the unfiltered SWNT suspensions serve as the source for assembly of functional RNPs and cleavage of the template DNA. Importantly, the Cas9 in vitro activity confirms that sgRNA, crRNA and tracrRNA remain intact and functional after our suspension protocols described in Figure 17.

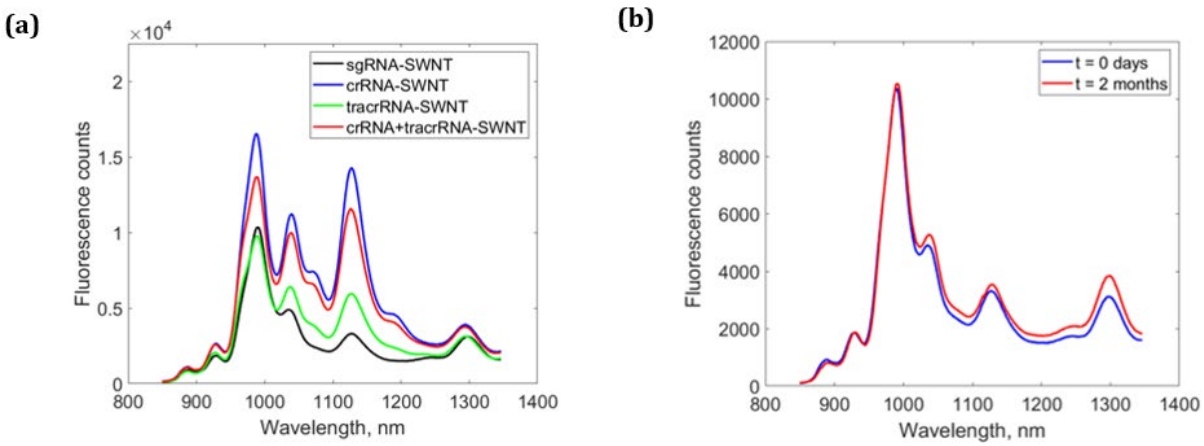

Figure 18. Near-infrared (nIR) fluorescence emission spectra of guide RNA-SWNTs. (A) Emission spectra of all spin-filtered guide RNA-SWNT formulations confirms individually suspended SWNTs are present in each formulation. (B) Comparison of emission spectra for spin-filtered sgRNA-SWNT at t = 0 days since preparation and t = 2 months since preparation demonstrates the stability of guide RNA SWNTs over time when stored at 4 ^{o}C. Spectra shown in (B) is representative of stability for all guide RNA SWNT formulations shown in (A).

Next, we investigated Cas9 in vitro activity for SWNT suspensions in the presence of Plant Cell Lysate (CL). Upon introduction to a plant cell, RNA must desorb from the SWNT surface in order to bind Cas9 and trigger targeted cleavage in the host genome. We hypothesize that proteins and other biomolecules present in a complex biofluid could promote guide RNA (sgRNA, crRNA/tracrRNA) desorption and lead to assembly of functional RNPs that would then successfully cleave template DNA. Figure 19B shows that unfiltered SWNT suspensions led to template DNA cleavage when incubated with Cas9 in Cas9 Buffer (B) or Plant Cell Lysate (CL) (Fig. 19B, Lanes 7 to 10). As for filtered SWNT suspensions, while incubation in Cas9 Buffer did not lead to template DNA cleavage (Fig. 19B, Lanes 11 and 13), incubation in Plant cell lysate led to template DNA cleavage (Fig. 19B, Lanes 12 and 14) indicating that sgRNA and crRNA/tracrRNA can be desorbed by cellular contents and lead to assembly of functional RNPs.

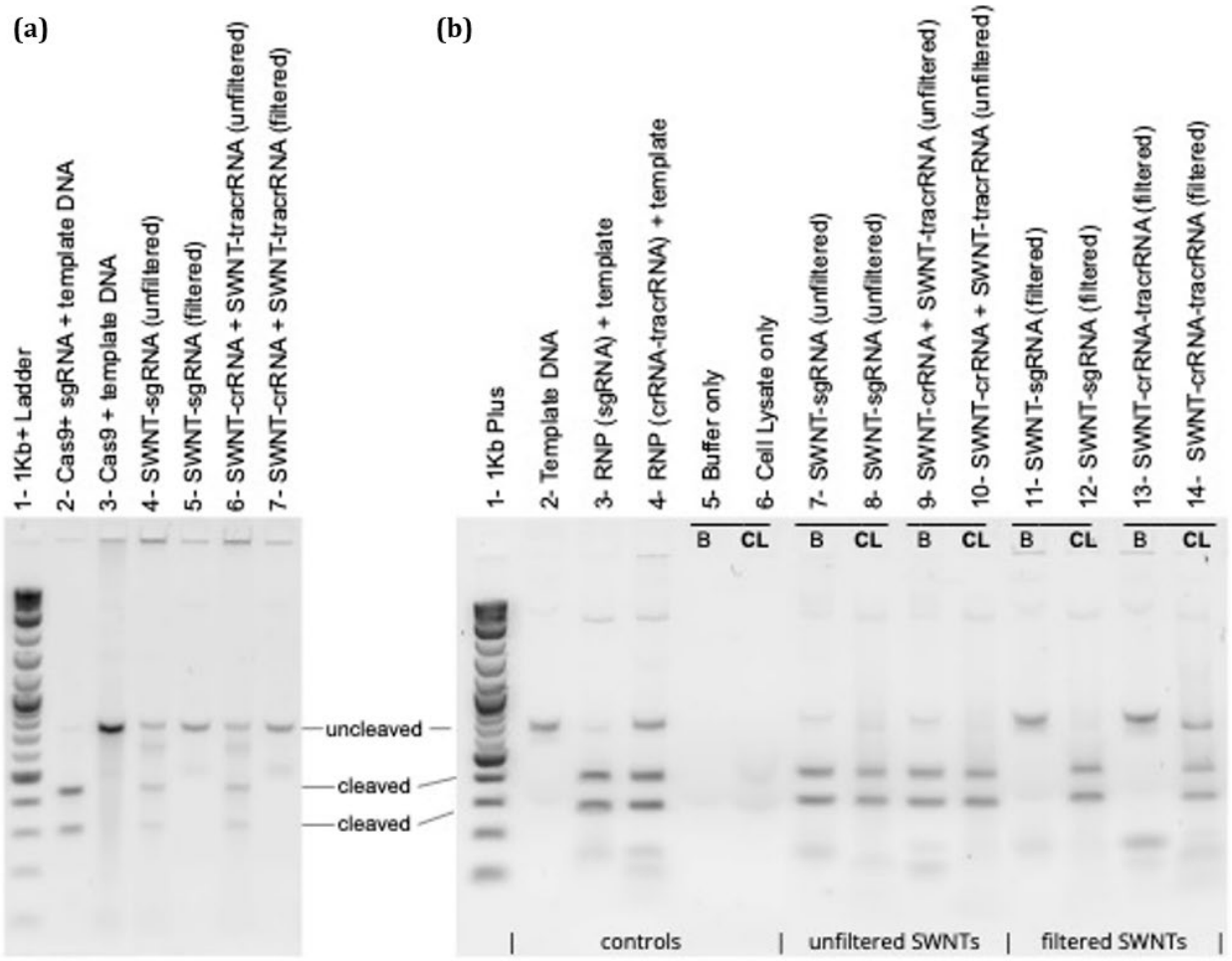

Figure 19. SpCas9 in vitro cleavage assay with guide RNA-SWNTs (sgRNA, crRNA and/or tracrRNA). (A) The functionality of guide RNAs post-sonication and loading onto SWNTs is investigated by combining SWNT suspensions with SpCas9 protein in Cas9 Buffer, DNA template, and incubated at 37°C for 8 hours. Cas9 in vitro reactions with filtered SWNT suspensions led to DNA template cleavage, while filtered SWNT suspensions did not. (B) Cas9 in vitro reactions with filtered SWNT suspensions incubated with Plant Cell Lysate led to cleavage of template DNA indicating desorption of guide RNAs (sgRNA or crRNA and tracrRNA) from SWNTs and assembly of functional RNPs.

To further investigate the desorption of gRNA through the formation of a biomolecular corona, wherein adsorbed RNA undergoes competitive binding with other molecules that have some affinity to the SWNT surface, we utilized a fluorescence-based assay previously developed in our lab[47] to measure the extent of RNA desorption when incubated in plant cell lysate containing a complex mixture of proteins and other biomolecules. In this assay, fluorescently-labeled ATTO550-tracrRNA was assembled with SWNTs with the resulting suspension showing no ATTO550 emission signal due to strong quenching caused by proximity to the nanotube surface (Figure 20A). However, upon

incubation in plant cell lysate from Nicotiana benthamiana protoplasts, ATTO550 signal is recovered due to RNA desorption from SWNTs promoted by competitive protein adsorption (Fig. 20A). Compared to a control protein fibrinogen, which is known to promote desorption of nucleic acids from SWNTs,[47] ATTO550-tracrRNA-SWNTs show a similar dose-dependent response in plant cell lysate (Fig. 20A), suggesting that complex biofluids such as those found inside plant cells would promote a significant proportion of RNA to become free for binding to Cas9. Furthermore, we found that the nIR fluorescence emission spectra of sgRNA-SWNTs exhibit a strong turn-on response in the presence of purified Cas9 protein (Fig. 20B). Due to intrinsic quenching from surface interactions between SWNTs and aromatic nucleic acid groups, nIR fluorescence turn-on of DNA/RNA-SWNTs in response to an analyte is a phenomena that is often suggestive of partial desorption of oligonucleotides adsorbed to the nanotube surface. Thus, the strong turn-on response of sgRNA-SWNTs in response to Cas9 suggests that Cas9 itself, in addition to endogenous proteins in the plant cell, could promote desorption of RNA from SWNTs.

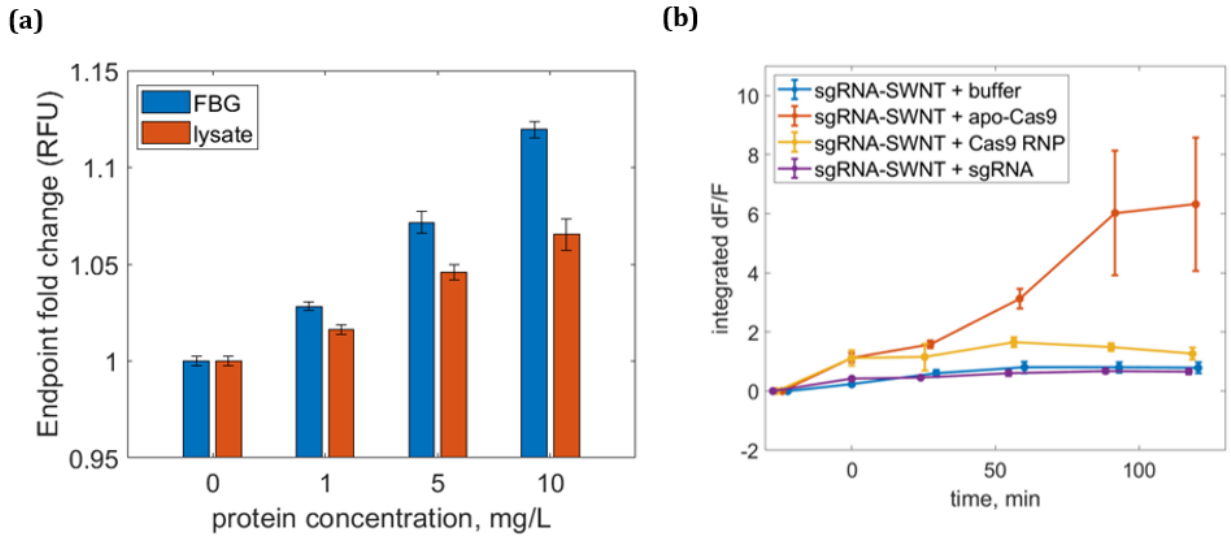

Figure 20. Protein-assisted desorption of guide RNA from SWNTs. (A) Using a fluorescence-based corona exchange assay described previously[47], desorption of labeled ATTO550-tracrRNA from SWNTs is measured by the recovery of ATTO550 emission signal when SWNTs are incubated with protein or in complex biofluid. FBG = fibrinogen, lysate = cell lysate from N. benthamiana protoplasts. (B) near-infrared (nIR) fluorescence emission response of filtered sgRNA-SWNTs, shown as the integrated spectra after analyte addition normalized to integrated spectra prior to analyte addition. A turn-on response (e.g. increase in integrated nIR emission) is indicative of desorption of sgRNA from SWNTs and a subsequent reduction in quenching of SWNT nIR photoluminescence caused by RNA adsorption. Analyte key: Buffer = 20 mM HEPES pH 7, 150 mM NaCl, apo-Cas9 = Cas9 without sgRNA, Cas9 RNP = Cas9 pre-complexed with sgRNA prior to addition, sgRNA = single guide RNA.

12. Conclusions

The development of a nanomaterial system for delivery of CRISPR gene editing cargo to mature plant tissue has great potential to address limitations in current biomolecule delivery methods, namely low efficiency, species/tissue limitations, host integration, and lack of novel systems for RNP delivery. In this work, we present strategies to address these limitations through the adaptation of PEI-SWNTS for plasmid delivery, and the development of a novel functionalization strategies for RNP and sgRNA delivery. A longterm goal of this work is to expand these biomolecular delivery systems towards applications in differentiable plant tissue, in order to address significant barriers in tissue regeneration that currently hinder widespread applications of CRISPR in plants. For most species, creating a stable gene-edited plant calls for an arduous, inefficient process of selection and regeneration of edited cells from tissue culture into a whole plant. This tissue culture requirement stems from inefficient, untargeted delivery tools but faces a significant disadvantage in that many species remain recalcitrant to regeneration, and those species that can be regenerated often do so inefficiently (<1-10% success rate). Thus, efficient direct targeting of differentiable tissue – meristems, flowers, pollen, embryos, or seeds - represents a 'holy grail' for an ideal delivery technology, and a goal that may be achievable via passive nanomaterial-mediated delivery.

13. CRISPR Methodology

Methodologies shared across chapters in this work are presented below.

13.1 CRISPR Target Design and Vector Construction

For GFP-targeting sgRNAs, guide sequence design was done referencing mGFP5 (Table 1). From the subset of PAM sites within mGFP5 that also contain a restriction site with a commercially available restriction enzyme, three locations were selected that were closest to the 5' end of the gene (EagI, MscI, and NdeI sites). The 20 nt spacers were designed to contain a restriction cleavage site at the expected cut site of Cas9 (2-3 bp PAM distal). Target sequences were also checked for off-targets by a BLAST query against the *N. benthamiana* draft genome v1.0.1 and found to have no matches in the wildtype genome. Baseline activity of each sgRNA was confirmed by an *in vitro* cleavage assay in which purified Cas9 and sgRNA were incubated with a PCR product amplified from genomic DNA isolated from the GFP transgenic *N. benthamiana* line (data not shown).

After *in* vitro verification of sgRNA-mediated Cas9 cleavage at the expected target sites, the spacer sequences were then cloned into individual plasmid vectors expressing both Cas9 and sgRNA. Complementary oligonucleotides containing the spacer sequences as well as 40 bp overhangs for Gibson Assembly into a parent vector (pJKW0457) were designed and ordered. pJKW0457 contains the sgRNA scaffold driven by the U6 scRNA promoter from *Arabidopsis thaliana* (AtU6), two BbsI sites to release a dummy 20 nt spacer by linearization, and a pUC18 backbone. 1 ug of pJKW0457 was linearized (and the dummy spacer released) by BbsI digestion. The spacer sequences were then cloned into linearized pJKW0457 by Gibson Assembly and transformed into competent *E. coli* cells for selection on ampicillin-containing solid media. Transformants were selected by colony PCR using spacer-specific primers to screen out religated parent plasmid. These intermediate plasmids containing

AtU6-sgRNA inserts (Table 1) were amplified in *E. coli* and purified for further cloning and Sanger sequencing to verify fragment insertion. A gene fragment containing spCas9-NLS driven by 35S promoter from *Cauliflower mosaic virus* was isolated from a parent vector (pJKW0458) by triple digestion with SbfI, EcoRI, and NheI followed by gel purification of the linear fragment of interest. The intermediate AtU6-sgRNA plasmids were double digested with EcoI and SbfI followed by gel purification of the linear fragment of interest. The AtU6-sgRNA fragments were then ligated with the 35S:Cas9 parent fragment and transformed into *E. coli* for selection on kanamycin-containing solid media. Transformants were selected by colony PCR with primers spanning the ligation site and the correct insert sequences verified by Sanger sequencing after plasmid amplification in *E. coli*. These final CRISPR vectors containing both AtU6-sgRNA and 35S:Cas9 were amplified to ~50 ug amounts to generate an excess of material for conjugation to PEI-SWNTs and subsequent leaf infiltration.

13.2 Delivery Conjugate Assembly and Leaf Infiltration

In general, CRISPR-SWNT delivery conjugates for leaf infiltration were prepared by coincubation of functionalized SWNT and biomolecular cargo (CRISPR vectors or preassembled Cas9 RNP) in buffer for 10 minutes at room temperature. Plasmid-PEI-SWNT conjugates were prepared at a 1:1 mass ratio of SWNT:DNA in 100 uL of plasmid infiltration buffer (20 mM MES pH 6, 60 mM $MgCl_2$). DNA delivery conjugates were prepared at different dosages of total plasmid: 1 ug and 2.5 ug plasmid, corresponding to PEI-SWNT concentrations of 10 mg/L and 25 mg/L. RNP-peptoid-SWNT conjugates were prepared in 100 uL of RNP infiltration buffer (20 mM HEPES pH 7.4, 150 mM NaCl) at variable molar ratios of Cas9:SWNT (10:1, 100:1, 500:1) while holding the SWNT concentration constant at 5 mg/L. Note that this approach of changing the molar ratio of Cas9:SWNT while holding the SWNT concentration constant results in a variable dosage of Cas9 RNP.

Upon assembly, CRISPR-SWNT delivery constructs were infiltrated into healthy, fully developed leaves of 3-4 week old *N. benthamiana* plants. To bypass the waxy cuticle, a small wound was first created using a pipette tip to create an indentation on the underside of a leaf (i.e. leaf abaxis). 100 uL of SWNT-cargo assembly suspension was drawn through a needle into a syringe. The needle was then removed and the suspension manually forced into the leaf through syringe expulsion at the wound location. During infiltration, liquid perfuses throughout the leaf tissue and the total wetted area becomes immediately visible. If the wetted area did not spread to the entire leaf by a single infiltration, additional infiltrations were performed to perfuse the entire leaf.

12.3 Genomic DNA Isolation and Target Amplification

7 days after infiltration with CRISPR-SWNT conjugates, genomic DNA was isolated from the entire leaf by CTAB extraction. Leaves were excised from the plant, folded into a screwcap conical vial containing lysis beads, and flash frozen in liquid nitrogen. Flash-frozen tissue was then ground into fine powder using a beadbeater machine. Powdered leaf tissue was submerged in 300 uL of CTAB buffer (2% Cetyltrimethyl ammonium bromide, 100 mM Tris HCl pH 8, 20 mM EDTA, 1.4 M NaCl, 1% polyvinylpyrollidone) and incubated at 65 C for

45 minutes to lyse the cells. To separate proteins and organic-soluble components, cell lysate was then diluted with 1 volume of 39:1 chloroform:isopropanol, vortexed, and centrifuged at 13,000 xg for 10 minutes. ~90% of the upper aqueous phase was then extracted and diluted with 1 volume of isopropanol to precipitate genomic DNA. After a 5 minute incubation at room temperature, a DNA pellet was collected by centrifugation at 13,000 xg for 10 minutes and removal of the supernatant. The pellet was then washed x3 with 100 uL ice-cold ethanol and resuspended in 30 uL water. Target locus amplification from genomic DNA then proceeded by PCR using gene-specific primers (Table 1) and PrimeSTAR GXL DNA polymerase. To measure cellular gene editing in proximity to the infiltration site, a small tissue sample (~2 mm) was collected from near the infiltration site and amplified directly using the MyTaq Plant PCR kit. Amplicons from both mGFP5 and PDS loci were ~800 bp in length and contained the sgRNA target sequence (and expected cut site) close to the center of the amplicon. Purified amplicons were then sent to Sanger sequencing and the resultant chromatograms were run through the Tracking Indels by DEcomposition (TIDE) sequence analysis algorithm.

Tables

Table 1. DNA sequences

mGFP5	ATGAAGACTAATCTTTTTCTCTTTCTCAT CTTTTCACTTCTCCTATCATTATCCTCGG CCGAATTCAGTAAAGGAGAAGAACTTTT CACTGGAGTTGTCCCAATTCTTGTTGAAT TAGATGGTGATGTTAATGGGTACAAATT TTCTGTCAGTGGAGAGGGTGAAGGTGAT GCAACATACGGAAAACTTACCCTTAAATT TATTTGCACTACTGGAAAACTACCTGTTC CATGGCCAACACTTGTCACTACTTTCTCT TATGGTGTTCAATGCTTTTCAAGATACCC AGATCATATGAAGCGGCACGACTTCTTCA AGAGCGCCATGCCTGAGGGATACGTGCAG GAGAGGACCATCTTCTTCAAGGACGACGG GAACTACAAGACACGTGCTGAAGTCAAG TTTGAGGGAGACACCCTCGTCAACAGGAT CGAGCTTAAGGGAATCGATTTCAAGGGG GACGGAAACATCCTCGGCCACAAGTTGGA ATACAACTACAACTCCCACAACGTATACA TCATGGCCGACAAGCAAAAGAACGGCATC AAAGCCAACTTCAAGACCCGCCACAACAT CGAAGACGGCGGCGTGCAACTCGCTGATC ATTATCAACAAAATACTCCAATTGGCGAT GGCCCTGTCCTTTTACCAGACAACCATTA CCTGTCCACACAATCTGCCCTTTCGAAAG ATCCCAACGAAAAGAGAGACCACATGGTC CTTCTTGAGTTTGTAACAGCTGCTGGGAT TACACATGGCATGGATGAACTATACAAA CATGATGAGCTTTAA
GFP sgRNA spacer, gRNA 208	TGGCCAACACTTGTCACTAC
GFP sgRNA spacer, gRNA 207	CGGCCGAATTCAGTAAAGGA
GFP sgRNA spacer, gRNA 206	GATACCCAGATCATATGAAG
AtU6:gRNA 206	TCGTTGAACAACGGAAACTCGACTTGCCT TCCGCACAATACATCATTTCTTCTTAGCT TTTTTTCTTCTTCTTCGTTCATACAGTTT TTTTTTGTTTATCAGCTTACATTTTCTTG AACCGTAGCTTTCGTTTTCTTCTTTTTAA CTTTCCATTCGGAGTTTTTGTATCTTGTT TCATAGTTTGTCCCAGGATTAGAATGATT AGGCATCGAACCTTCAAGAATTTGATTGA ATAAAACATCTTCATTCTTAAGATATGA AGATAATCTTCAAAAGGCCCCTGGGAATC TGAAAGAAGAGAAGCAGGCCCATTTATA

	TGGGAAAGAACAATAGTATTTCTTATAT AGGCCCATTTAAGTTGAAAACAATCTTCA AAAGTCCCACATCGCTTAGATAAGAAAAC GAAGCTGAGTTTATATACAGCTAGAGTC GAAGTAGTGATTGATACCCAGATCATAT GAAGGTTTTAGAGCTAGAAATAGCAAGT TAAAATAAGGCTAGTCCGTTATCAACTTG AAAAAGTGGCACCGAGTCGGTGCTTTTTT T
AtU6:gRNA 207	TCGTTGAACAACGGAAACTCGACTTGCCT TCCGCACAATACATCATTTCTTCTTAGCT TTTTTTCTTCTTCTTCGTTCATACAGTTT TTTTTTGTTTATCAGCTTACATTTTCTTG AACCGTAGCTTTCGTTTTCTTCTTTTTAA CTTTCCATTCGGAGTTTTTGTATCTTGTT TCATAGTTTGTCCCAGGATTAGAATGATT AGGCATCGAACCTTCAAGAATTTGATTGA ATAAAACATCTTCATTCTTAAGATATGA AGATAATCTTCAAAAGGCCCCTGGGAATC TGAAAGAAGAGAAGCAGGCCCATTTATA TGGGAAAGAACAATAGTATTTCTTATAT AGGCCCATTTAAGTTGAAAACAATCTTCA AAAGTCCCACATCGCTTAGATAAGAAAAC GAAGCTGAGTTTATATACAGCTAGAGTC GAAGTAGTGATTGTCCTTTACTGAATTCG GCCGGTTTTAGAGCTAGAAATAGCAAGT TAAAATAAGGCTAGTCCGTTATCAACTTG AAAAAGTGGCACCGAGTCGGTGCTTTTTT T
AtU6:gRNA 208	TCGTTGAACAACGGAAACTCGACTTGCCT TCCGCACAATACATCATTTCTTCTTAGCT TTTTTTCTTCTTCTTCGTTCATACAGTTT TTTTTTGTTTATCAGCTTACATTTTCTTG AACCGTAGCTTTCGTTTTCTTCTTTTTAA CTTTCCATTCGGAGTTTTTGTATCTTGTT TCATAGTTTGTCCCAGGATTAGAATGATT AGGCATCGAACCTTCAAGAATTTGATTGA ATAAAACATCTTCATTCTTAAGATATGA AGATAATCTTCAAAAGGCCCCTGGGAATC TGAAAGAAGAGAAGCAGGCCCATTTATA TGGGAAAGAACAATAGTATTTCTTATAT AGGCCCATTTAAGTTGAAAACAATCTTCA AAAGTCCCACATCGCTTAGATAAGAAAAC GAAGCTGAGTTTATATACAGCTAGAGTC GAAGTAGTGATTGTAGTGACAAGTGTTG

	GCCAGTTTTAGAGCTAGAAATAGCAAGT TAAAATAAGGCTAGTCCGTTATCAACTTG AAAAAGTGGCACCGAGTCGGTGCTTTTTT T
35S:hcoCas9	tgagacttttcaacaaagggtaatatcgggaaacctcct cggattccattgcccagctatctgtcacttcatcaaaagg acagtagaaaaggaaggtggcacctacaaatgccatc attgcgataaaggaaaggctatcgttcaagatgcctctg ccgacagtggtcccaaagatggacccccacccacaagg agcatcgtggaaaaagaagacgttccaaccacgtcttc aaagcaagtggattgatgtgatatctccactgacgtaag ggatgacgcacaatcccactatccttcgccccaagcttg ggcccaagcttgggtcgcgccccacggatggtataaga ataaaggcattccgcgtgcaggattcacccgttcgcctc tcacctttcgctgtactctctcgccacacacacccctct ccagctccgttggagctccggacagcagcaggcgcggg gcggtcacgtagtaagcagctctcggctccctctcccctt gctccgtggatccatggattacaaggatgatgatgataa ggattacaaggatgatgatgataagatggctccaaaga agaagagaaaggttggaatccacggagttccagctgct gataagaagtactctatcggacttgacatcggaaccaa ctctgttggatgggctgttatcaccgatgagtacaaggtt ccatctaagaagttcaaggttcttggaaacaccgataga cactctatcaagaagaaccttatcggtgctcttcttttcga ttctggagagaccgctgaggctaccagattgaagagaa ccgctagaagaagatacaccagaagaaagaacagaat ctgctaccttcaggaaatcttctctaacgagatggctaa ggttgatgattctttcttccacagacttgaggagtctttcc ttgttgaggaggataagaagcacgagagacacccaatc ttcggaaacatcgttgatgaggttgcttaccacgagaag tacccaaccatctaccaccttagaaagaagttggttgatt ctaccgataaggctgatcttagacttatctaccttgctctt gctcacatgatcaagttcagaggacacttccttatcgag ggagaccttaacccagataactctgatgttgataagttgt tcatccagcttgttcagacctacaaccagcttttcgagga gaacccaatcaacgcttctggagttgatgctaaggctat cctttctgctagactttctaagtctcgtagacttgagaacc ttatcgctcagcttccaggagagaagaagaacggacttt tcggaaaccttatcgctctttctcttggacttaccccaaac ttcaagtctaacttcgatcttgctgaggatgctaagttgc agctttctaaggatacctacgatgatgatcttgataacct tcttgctcagatcggagatcagtacgctgatcttttccttg ctgctaagaacctttctgatgctatccttctttctgacatc cttagagttaacaccgagatcaccaaggctccactttct gcttctatgatcaagagatacgatgagcaccaccagga

	tcttacccttttgaaggctcttgttagacagcagcttccag agaagtacaaggaaatcttcttcgatcagtctaagaacg gatacgctggatacatcgatggaggagcttctcaggag gagttctacaagttcatcaagccaatccttgagaagatg gatggaaccgaggagcttcttgttaagttgaacagaga ggatcttcttagaaagcagagaaccttcgataacggatc tatcccacaccagatccaccttggagagcttcacgctat ccttcgtagacaggaggatttctacccattcttgaaggat aacagagagaagatcgagaagatccttaccttcagaat cccatactacgttggaccacttgctagaggaaactctcg tttcgcttggatgaccagaaagtctgaggagaccatcac cccttggaacttcgaggaggtaagtttctgcttctacctttt gatatatatataataattatcattaattagtagtaatataa tatttcaaatatttttttcaaaataaaagaatgtagtatat agcaattgcttttctgtagtttataagtgtgtatattttaat ttataacttttctaatatatgaccaaaatttgttgatgtgc aggttgttgataagggagcttctgctcagtctttcatcga gagaatgaccaacttcgataagaaccttccaaacgaga aggttcttccaaagcactctcttctttacgagtacttcacc gtttacaacgagcttaccaaggttaagtacgttaccgag ggaatgagaaagccagctttcctttctggagagcagaa gaaggctatcgttgatcttcttttcaagaccaacagaaa ggttaccgttaagcagttgaaggaggattacttcaagaa gatcgagtgcttcgattctgttgaaatctctggagttgag gatagattcaacgcttctcttggaacctaccacgatctttt gaagatcatcaaggataaggatttccttgataacgagg agaacgaggacatccttgaggacatcgttcttaccctta ccctttttcgaggatagagagatgatcgaggagagactc aagacctacgctcacctttttcgatgataaggttatgaag cagttgaagagaagaagatacaccggatggggtagac tttctcgtaagttgatcaacggaatcagagataagcagt ctggaaagaccatccttgatttcttgaagtctgatggatt cgctaacagaaacttcatgcagcttatccacgatgattct cttaccttcaaggaggacatccagaaggctcaggtttct ggacagggagattctcttcacgagcacatcgctaacctt gctggatctccagctatcaagaagggaatccttcagacc gttaaggttgttgatgagcttgttaaggttatgggtagac acaagccagagaacatcgttatcgagatggctagagag aaccagaccacccagaagggacagaagaactctcgtg agagaatgaagagaatcgaggagggaatcaaggagct tggatctcaaatcttgaaggagcacccagttgagaaca cccagcttcagaacgagaagttgtacctttactaccttca gaacggaagagatatgtacgttgatcaggagcttgaca tcaacagactttctgattacgatgttgatcacatcgttcc acagtctttcttgaaggatgattctatcgataacaaggtt

	cttacccgttctgataagaacagaggaaagtctgataac gttccatctgaggaggttgttaagaagatgaagaactac tggagacagcttcttaacgctaagttgatcacccagaga aagttcgataaccttaccaaggctgagagaggaggact ttctgagcttgataaggctggattcatcaagagacagct tgttgagaccagacagatcaccaagcacgttgctcagat ccttgattctcgtatgaacaccaagtacgatgagaacga taagttgatcagagaggttaaggttatcaccttgaagtct aagttggtttctgatttcagaaaggatttccagttctaca aggttagagagatcaacaactaccaccacgctcacgat gcttaccttaacgctgttgttggaaccgctcttatcaaga agtacccaaagttggagtctgagttcgtttacggagatt acaaggtttacgatgttagaaagatgatcgctaagtctg agcaggagatcggaaaggctaccgctaagtacttcttct actctaacatcatgaacttcttcaagaccgagatcaccct tgctaacggagagatcagaaagagaccacttatcgaga ccaacggagagaccggagagatcgtttgggataaggg aagagatttcgctaccgttagaaaggttctttctatgcca caggttaacatcgttaagaaaaccgaggttcagaccgg aggattctctaaggagtctatccttccaaagagaaactc tgataagttgatcgctagaaagaaggattgggacccaa agaagtacggaggattcgattctccaaccgttgcttact ctgttcttgttgttgctaaggttgagaagggaaagtctaa gaagttgaagtctgttaaggagcttcttggaatcaccat catggagcgttcttctttcgagaagaacccaatcgatttc cttgaggctaagggatacaaggaggttaagaaggatct tatcatcaagttgccaaagtactctcttttcgagcttgag aacggaagaaagagaatgcttgcttctgctggagagct tcagaagggaaacgagcttgctcttccatctaagtacgt taacttcctttaccttgcttctcactacgagaagttgaag ggatctccagaggataacgagcagaagcagcttttcgtt gagcagcacaagcactaccttgatgagatcatcgagca aatctctgagttctctaagagagttatccttgctgatgcta accttgataaggttctttctgcttacaacaagcacagag ataagccaatcagagagcaggctgagaacatcatccac cttttcacccttaccaaccttggtgctccagctgctttcaa gtacttcgataccaccatcgatagaaaaagatacacctc taccaaggaggttcttgatgctacccttatccaccagtct atcaccggactttacgagaccagaatcgatctttctcag cttggaggagataagagaccagctgctaccaagaagg ctggacaggctaagaagaagaag
Phyotene desaturase (PDS), *Nicotiana benthamiana*	GAATGAGCAAAGCAAGAAATTAAAAAGA GAGAGAGGTGCTTTATCCATCAAATGTG GCTATGGTAGGAAGAGCCAATGGTGGGA CATTTTTGGAGTGTAGCCAAAACATAAA

	GGAAGGTCCAGTGCGAGTTACTGCAAATT GAGTTGGGAGTGAGGATTAAAGAAGATA GTAACATATTTCTAGCTAAATAGCAAAC AAATGATCCGTTAACAGAAGTGGCCAAA CCACCAAATTCAGGCATCTCCACCAAATA TTAGTTTTTTATACACAAAAGATTCAAC ACAAACAGTTAAGTACTTCTTTAATCGTT CCTAATTCTTTGTTCAGGGGTATCTTTTT GTGGGTAACGGCCAAACCACCACAAATTT TCAGTTCCCACTCTTAACTCTTTCAACTT CAACACAACAAATTAGTATTTGCTTTTCC TTCTTTGCTTATCTAGTGCATAACGATTT TCTACAACTTTAGCATAGTCCACAACGTG AAACACAACTCCTTGGCGGTTTATACCGA GGTAAGAAATGATTTTGGTTTCTTTGGT TACATCAGCTGAATGCTTTGCTTGAGAAA AGCTCTCTTTTTCCCGTTTAGGATCTTGT TTATTTGCTTTCGTTTTTCTACTCGTTTG AATTTTAACTTGATTTTGTGGGTGAAGG CTAATTTTTCTCATAGTGTAAGAACAAGT TTCATATGTACTGTAAAAGCTAGAATCTT TTTTACTTTTGCATATAAATTTGTGTAAT AAATGCTTAAGAACCAGAATATTTGAAA AAGATAAGGAATTTTGCATAGTATTTAG GTTCACAAGTGGGACAATCTTCTTACACT GAAATATCTTTATGTCAGGCTTAATTTAC TGCTATCTTGTTCAATAAAATGCCCCAAA TTGGACTTGTTTCTGCCGTTAATTTGAGA GTCCAAGGTAATTCAGCTTATCTTTGGAG CTCGAGGTCTTCGTTGGGAACTGAAAGTC AAGATGTTTGCTTGCAAAGGAATTTGTT ATGTTTTGGTAGTAGCGACTCCATGGGGC ATAAGTTAAGGATTCGTACTCCAAGTGCC ACGACCCGAAGATTGACAAAGGACTTTA ATCCTTTAAAGGTTTGTTTTGAATGCGAA AGTGTGATGCTGGATTTATGATCGTGGGC ATATATCCTCTAAAATAAGAGATGTATA TCTTGCCATTCAGGTAGTCTGCATTGATT ATCCAAGACCAGAGCTAGACAATACAGTT AACTATTTGGAGGCGGCGTTATTATCATC ATCGTTTCGTACTTCCTCACGCCCAACTA AACCATTGGAGATTGTTATTGCTGGTGCA GGTGATTTTTTCCAGCCATCTATATTTGT AGTTTTCATTTTTCTTTCTTTGGAAGGAA GATCATTCTATTAGTTATATTATCACTAG

	AATATTTACCTGTACATTCTTTTCTGATT AACTGTTTTGGACCGCAAAATTTTAGGTT CTTACTTCTTCGCCATTTTGCAACTAATC AGCAATTAGGAGCGGTTTGAAAACTAGT TTGTTTTGAACTATTTTTGCCGTCACTCT ATTTATATACTGTTGAATTGTCCCAAATC GGTGGAATTTGAGGTCCTTGG
PDS sgRNA spacer	GCCGTTAATTTGAGAGTCCA
mGFP5 forward primer for TIDE analysis	GATGACGCACAATCCCACTATC
mGFP5 reverse primer for TIDE analysis	AGGACCATGTGGTCTCTCTTT
PDS forward primer for TIDE analysis	CAGCTGAATGCTTTGCTTGA
PDS reverse primer for TIDE analysis	ATGGTTTAGTTGGGCGTGAG

Table 2. Selected protein delivery studies in plants.

Carrier	Species and tissue type	Protein Cargo	Delivery Method	Method of Validation	Ref.
Biolistic delivery in walled plant cells					
Au-capped MSNs	Onion epidermis, tobacco leaves, teosinte leaves	FITC/TRITC-BSA, GFP	Biolistic	Widefield FL microscopy	[52]
Au-capped MSNs	Maize embryos	Cre recombinase	Biolistic	Widefield FL microscopy, southern blot (1-20% T0 recombinants)	[63]
Au microparticles	Onion epidermis, tobacco leaves	GFP, dsRed, BSA-TRITC, GUS, RNAse A, trypsin	Biolistic	Widefield FL microscopy	[10]
Au microparticles	Maize embryos	Cas9 RNP	Biolistic	Amplicon deep sequencing (2-9% mutated T0 progeny)	[64]
Au particles + cationic lipid	Rice embryos	Cas9 RNPs + hygR selection plasmid	Biolistic	Sanger sequencing (63% of selected transformants carried mutations)	[65]
Au particles	Rice embryos	Cas9 and Cas12a RNPs + hygR selection plasmid	Biolistic	NGS (3% WT Cas9, 9% HiFi Cas9, 32% Cas12a)	[66]
Peptide-mediated transfection in walled plant cells					
AID peptide complexes	Onion and tomato roots, onion epidermis	GFP, RFP	Incubation with protein-peptide solution	Confocal FL microscopy	[67]
Tat PTD and R9 AID peptide complexes	Onion and maize roots, onion epidermis	GFP, RFP	Incubation with protein-peptide solution	Confocal FL microscopy	[68]
R9 AID peptide complexes	Onion roots	GFP, RFP (covalent and noncovalent codelivery)	Incubation with protein-peptide solution	Confocal FL microscopy	[69]
TpI CPP complexes	Wheat and rapeseed roots and protoplasts	GUS	Incubation with protein-peptide solution	Confocal FL microscopy, GUS fluorometric analysis	[70]
BP100(KH)9 and BP100CH7 CPP complexes	Rice callus	YFP	Vacuum infiltration	Confocal FL microscopy	[7]
2BP100-K8 CPP fusion	Apple leaves	Neomycin phosphotransferase II (NPTII)	Leaf infiltration	Confocal FL microscopy	[8]
(BP100)2K8 and BP100(KH)9 CPP fusion	Arabidopsis leaves	BSA-RhB, ADH-RhB, YFP	Leaf infiltration	Confocal FL microscopy	[48]
Electroporation in walled plant cells					

-	Tobacco BY2 culture	ERD14 and ERD10 intrinsically disordered proteins (IDPs)	Electroporation	Confocal FL microscopy	[71]
-	Arabidopsis T87 culture	Cre recombinase	Electroporation	GUS fluorometric analysis, genomic PCR	[72]
Protoplast transfection					
PEG	Arabidopsis, tobacco, rice, lettuce protoplasts	Cas9 RNP	PEG transfection	T7E1 (44% mutation rate), RFLP (46% mutation rate)	[73]
PEG	Tobacco protoplasts	GFP, I-SceI meganuclease + YFP positive selection plasmid, Host-targeting TALEN	PEG transfection	Flow cytometry (2.7% YFP expression) and 454 pyrosequencing (1.4% mutation rate)	[74]
PEG	Petunia protoplasts	Cas9 RNP	PEG transfection	T7E1 (2-20% mutation rate), amplicon deep sequencing (11.5 ± 2% mutation rate)	[75]
PEG	Grapevine and apple protoplasts	Cas9 RNP	PEG transfection	Amplicon deep sequencing (2-7% mutation rate)	[76]
PEG	Bread wheat protoplasts	Cas9 RNP	PEG transfection	RFLP, amplicon deep sequencing (2-4% mutated T0 progeny)	[77]
PEG	Potato protoplasts	Cas9 RNP	PEG transfection	Sanger sequencing (1-20% mutated T0 progeny)	[78]
Lipofectamine 3000	Tobacco BY2 protoplasts	Cas9 RNP	Liposome transfection	Widefield FL microscopy	[79]

Table 3. Selected nanoparticle delivery studies in plants.

	NP type	Cargo	Plant Species; Cell/Tissue type	Delivery Method	Comments	Ref., Year
With external aid	Gold-plated MSNs	GFP and mCherry plasmids; GFP protein	*Allium cepa* epidermis tissue	Biolistic	DNA and protein codelivery	[62], 2012
	Gold-plated MSNs	AmCyan1 and DsRed2 plasmids; Cre protein	*Zea mays* immature embryos	Biolistic	DNA and protein codelivery; both transient and stable expression	[63], 2014
	Poly-L-lysine coated starch NPs	GFP plasmid	*Dioscorea zingiberensis C.H.Wright* calli suspension	Sonoporation	5% transient expression efficiency; some integration occurred	[64], 2008
	Magnetic gold NPs	β-glucuronidase (GUS) plasmid	*Brassica napus* protoplasts and walled cell suspension	Magnetic field	Transient GUS expression	[65], 2013
	Dimethylaminoethyl methacrylate (DMAEM) polymer NPs	Yellow fluorescent protein (YFP) and GFP plasmids	*N. tabacum* and *Ceratodon purpureus* protoplasts	PEG transfection	Both transient expression and stable transformation	[66], 2017
	Magnetic Fe_3O_4 NPs	Selectable marker gene plasmids	*Gossypium hirsutum* pollen	Magnetic field	~1% efficiency of generating stable transgenic seeds	[67], 2017
***In vitro* without external aid**	Calcium phosphate NPs (CaPNPs)	GUS plasmid	*Brassica juncea* hypocotyl explants	Passive	80.7% stable transformation efficiency	[68], 2012
	Polyamidoamine (PAMAM) dendrimer NPs	GFP plasmid	*Agrostis stolonifera L.* calli	Passive	48.5% of cells showed transient expression	[69], 2008
***In vivo* without external aid**	PAMAM dendrimer NPs	Double-stranded DNA for RNA interference	*Arabidopsis thaliana* roots	Passive	Developmental gene silencing led to systemic phenotypes	[70], 2014

Organically functionalized MSNs	mCherry plasmid	*A. thaliana* roots	Passive	46.5% transient expression efficiency	[71], 2013
Organically functionalized CNTs	GFP plasmid; siRNA for transgenic GFP silencing	*Eruca sativa* and *Nicotiana benthamiana* leaves	Passive	95% transient silencing efficiency	

References

(1) Eliazer Nelson, A. R. L.; Ravichandran, K.; Antony, U. The Impact of the Green Revolution on Indigenous Crops of India. *Journal of Ethnic Foods* **2019**, *6* (1), 8. https://doi.org/10.1186/s42779-019-0011-9.

(2) Khush, G. S. *IR Varieties and Their Impact*; Int. Rice Res. Inst., 2005.

(3) Cunningham, F. J.; Goh, N. S.; Demirer, G. S.; Matos, J. L.; Landry, M. P. Nanoparticle-Mediated Delivery towards Advancing Plant Genetic Engineering. *Trends in Biotechnology* **2018**, *36* (9), 882–897. https://doi.org/10.1016/j.tibtech.2018.03.009.

(4) Ray, D. K.; Mueller, N. D.; West, P. C.; Foley, J. A. Yield Trends Are Insufficient to Double Global Crop Production by 2050. *PLOS ONE* **2013**, *8* (6), e66428. https://doi.org/10.1371/journal.pone.0066428.

(5) Shao, X.; Wu, S.; Dou, T.; Zhu, H.; Hu, C.; Huo, H.; He, W.; Deng, G.; Sheng, O.; Bi, F.; Gao, H.; Dong, T.; Li, C.; Yang, Q.; Yi, G. Using CRISPR/Cas9 Genome Editing System to Create MaGA20ox2 Gene-Modified Semi-Dwarf Banana. *Plant Biotechnology Journal 0* (0). https://doi.org/10.1111/pbi.13216.

(6) Zheng, M.; Zhang, L.; Tang, M.; Liu, J.; Liu, H.; Yang, H.; Fan, S.; Terzaghi, W.; Wang, H.; Hua, W. Knockout of Two BnaMAX1 Homologs by CRISPR/Cas9-Targeted Mutagenesis Improves Plant Architecture and Increases Yield in Rapeseed (Brassica Napus L.). *Plant Biotechnology Journal 0* (0). https://doi.org/10.1111/pbi.13228.

(7) Razzaq, A.; Saleem, F.; Kanwal, M.; Mustafa, G.; Yousaf, S.; Imran Arshad, H. M.; Hameed, M. K.; Khan, M. S.; Joyia, F. A. Modern Trends in Plant Genome Editing: An Inclusive Review of the CRISPR/Cas9 Toolbox. *International Journal of Molecular Sciences* **2019**, *20* (16), 4045. https://doi.org/10.3390/ijms20164045.

(8) Cai, Y.; Chen, L.; Liu, X.; Guo, C.; Sun, S.; Wu, C.; Jiang, B.; Han, T.; Hou, W. CRISPR/Cas9-Mediated Targeted Mutagenesis of GmFT2a Delays Flowering Time in Soya Bean. *Plant Biotechnology Journal* **2018**, *16* (1), 176–185. https://doi.org/10.1111/pbi.12758.

(9) Kim, H.; Kim, S.-T.; Ryu, J.; Kang, B.-C.; Kim, J.-S.; Kim, S.-G. CRISPR/Cpf1-Mediated DNA-Free Plant Genome Editing. *Nat Commun* **2017**, *8* (1), 1–7. https://doi.org/10.1038/ncomms14406.

(10) Sánchez-León, S.; Gil-Humanes, J.; Ozuna, C. V.; Giménez, M. J.; Sousa, C.; Voytas, D. F.; Barro, F. Low-Gluten, Nontransgenic Wheat Engineered with CRISPR/Cas9. *Plant Biotechnology Journal* **2018**, *16* (4), 902–910. https://doi.org/10.1111/pbi.12837.

(11) Zhang, Y.; Liang, Z.; Zong, Y.; Wang, Y.; Liu, J.; Chen, K.; Qiu, J.-L.; Gao, C. Efficient and Transgene-Free Genome Editing in Wheat through Transient Expression of CRISPR/Cas9 DNA or RNA. *Nat Commun* **2016**, *7* (1), 1–8. https://doi.org/10.1038/ncomms12617.

(12) Zhang, Y.; Li, D.; Zhang, D.; Zhao, X.; Cao, X.; Dong, L.; Liu, J.; Chen, K.; Zhang, H.; Gao, C.; Wang, D. Analysis of the Functions of TaGW2 Homoeologs in Wheat Grain Weight and

Protein Content Traits. *The Plant Journal* **2018**, *94* (5), 857–866. https://doi.org/10.1111/tpj.13903.

(13) Qi, W.; Zhu, T.; Tian, Z.; Li, C.; Zhang, W.; Song, R. High-Efficiency CRISPR/Cas9 Multiplex Gene Editing Using the Glycine TRNA-Processing System-Based Strategy in Maize. *BMC Biotechnology* **2016**, *16* (1), 58. https://doi.org/10.1186/s12896-016-0289-2.

(14) Li, T.; Yang, X.; Yu, Y.; Si, X.; Zhai, X.; Zhang, H.; Dong, W.; Gao, C.; Xu, C. Domestication of Wild Tomato Is Accelerated by Genome Editing. *Nature Biotechnology* **2018**, *36* (12), 1160–1163. https://doi.org/10.1038/nbt.4273.

(15) Zsögön, A.; Čermák, T.; Naves, E. R.; Notini, M. M.; Edel, K. H.; Weinl, S.; Freschi, L.; Voytas, D. F.; Kudla, J.; Peres, L. E. P. *De Novo* Domestication of Wild Tomato Using Genome Editing. *Nature Biotechnology* **2018**, *36* (12), 1211–1216. https://doi.org/10.1038/nbt.4272.

(16) Lemmon, Z. H.; Reem, N. T.; Dalrymple, J.; Soyk, S.; Swartwood, K. E.; Rodriguez-Leal, D.; Eck, J. V.; Lippman, Z. B. Rapid Improvement of Domestication Traits in an Orphan Crop by Genome Editing. *Nature Plants* **2018**, *4* (10), 766–770. https://doi.org/10.1038/s41477-018-0259-x.

(17) Zhan, X.; Zhang, F.; Zhong, Z.; Chen, R.; Wang, Y.; Chang, L.; Bock, R.; Nie, B.; Zhang, J. Generation of Virus-resistant Potato Plants by RNA Genome Targeting. *Plant Biotechnol J* **2019**, *17* (9), 1814–1822. https://doi.org/10.1111/pbi.13102.

(18) Gomez, M. A.; Lin, Z. D.; Moll, T.; Chauhan, R. D.; Hayden, L.; Renninger, K.; Beyene, G.; Taylor, N. J.; Carrington, J. C.; Staskawicz, B. J.; Bart, R. S. Simultaneous CRISPR/Cas9-mediated Editing of Cassava EIF4E Isoforms NCBP-1 and NCBP-2 Reduces Cassava Brown Streak Disease Symptom Severity and Incidence. *Plant Biotechnol J* **2019**, *17* (2), 421–434. https://doi.org/10.1111/pbi.12987.

(19) Wang, Y.; Cheng, X.; Shan, Q.; Zhang, Y.; Liu, J.; Gao, C.; Qiu, J.-L. Simultaneous Editing of Three Homoeoalleles in Hexaploid Bread Wheat Confers Heritable Resistance to Powdery Mildew. *Nature Biotechnology* **2014**, *32* (9), 947–951. https://doi.org/10.1038/nbt.2969.

(20) Kim, Y.-A.; Moon, H.; Park, C.-J. CRISPR/Cas9-Targeted Mutagenesis of Os8N3 in Rice to Confer Resistance to Xanthomonas Oryzae Pv. Oryzae. *Rice* **2019**, *12* (1), 67. https://doi.org/10.1186/s12284-019-0325-7.

(21) Bari, V. K.; Nassar, J. A.; Kheredin, S. M.; Gal-On, A.; Ron, M.; Britt, A.; Steele, D.; Yoder, J.; Aly, R. CRISPR/Cas9-Mediated Mutagenesis of CAROTENOID CLEAVAGE DIOXYGENASE 8 in Tomato Provides Resistance against the Parasitic Weed Phelipanche Aegyptiaca. *Sci Rep* **2019**, *9* (1), 1–12. https://doi.org/10.1038/s41598-019-47893-z.

(22) Mojica, F. J. M.; Díez-Villaseñor, C.; García-Martínez, J.; Soria, E. Intervening Sequences of Regularly Spaced Prokaryotic Repeats Derive from Foreign Genetic Elements. *J Mol Evol* **2005**, *60* (2), 174–182. https://doi.org/10.1007/s00239-004-0046-3.

(23) Jinek, M.; Chylinski, K.; Fonfara, I.; Hauer, M.; Doudna, J. A.; Charpentier, E. A Programmable Dual-RNA–Guided DNA Endonuclease in Adaptive Bacterial Immunity. *Science* **2012**, *337* (6096), 816–821. https://doi.org/10.1126/science.1225829.

(24) Jiang, F.; Doudna, J. A. CRISPR-Cas9 Structures and Mechanisms. *Annu Rev Biophys* **2017**, *46*, 505–529. https://doi.org/10.1146/annurev-biophys-062215-010822.

(25) Chandrasegaran, S.; Carroll, D. Origins of Programmable Nucleases for Genome Engineering. *Journal of Molecular Biology* **2016**, *428* (5, Part B), 963–989. https://doi.org/10.1016/j.jmb.2015.10.014.

(26) Zhang, H.; Goh, N. S.; Wang, J. W.; Pinals, R. L.; González-Grandío, E.; Demirer, G. S.; Butrus, S.; Fakra, S. C.; Del Rio Flores, A.; Zhai, R.; Zhao, B.; Park, S.-J.; Landry, M. P. Nanoparticle Cellular Internalization Is Not Required for RNA Delivery to Mature Plant Leaves. *Nat. Nanotechnol.* **2022**, *17* (2), 197–205. https://doi.org/10.1038/s41565-021-01018-8.

(27) Martin-Ortigosa, S.; Peterson, D. J.; Valenstein, J. S.; Lin, V. S.-Y.; Trewyn, B. G.; Lyznik, L. A.; Wang, K. Mesoporous Silica Nanoparticle-Mediated Intracellular Cre Protein Delivery for Maize Genome Editing via LoxP Site Excision,. *Plant Physiology* **2014**, *164* (2), 537–547. https://doi.org/10.1104/pp.113.233650.

(28) Martin-Ortigosa, S.; Valenstein, J. S.; Lin, V. S.-Y.; Trewyn, B. G.; Wang, K. Gold Functionalized Mesoporous Silica Nanoparticle Mediated Protein and DNA Codelivery to Plant Cells Via the Biolistic Method. *Advanced Functional Materials* **2012**, *22* (17), 3576–3582. https://doi.org/10.1002/adfm.201200359.

(29) Torney, F.; Trewyn, B. G.; Lin, V. S.-Y.; Wang, K. Mesoporous Silica Nanoparticles Deliver DNA and Chemicals into Plants. *Nature Nanotech* **2007**, *2* (5), 295–300. https://doi.org/10.1038/nnano.2007.108.

(30) Chang, F.-P.; Kuang, L.-Y.; Huang, C.-A.; Jane, W.-N.; Hung, Y.; Hsing, Y. C.; Mou, C.-Y. A Simple Plant Gene Delivery System Using Mesoporous Silica Nanoparticles as Carriers. *J. Mater. Chem. B* **2013**, *1* (39), 5279–5287. https://doi.org/10.1039/C3TB20529K.

(31) Liu, J.; Wang, F.; Wang, L.; Xiao, S.; Tong, C.; Tang, D.; Liu, X. Preparation of Fluorescence Starch-Nanoparticle and Its Application as Plant Transgenic Vehicle. *J. Cent. South Univ. Technol.* **2008**, *15* (6), 768–773. https://doi.org/10.1007/s11771-008-0142-4.

(32) Zhao, X.; Meng, Z.; Wang, Y.; Chen, W.; Sun, C.; Cui, B.; Cui, J.; Yu, M.; Zeng, Z.; Guo, S.; Luo, D.; Cheng, J. Q.; Zhang, R.; Cui, H. Pollen Magnetofection for Genetic Modification with Magnetic Nanoparticles as Gene Carriers. *Nature Plants* **2017**, *3* (12), 956–964. https://doi.org/10.1038/s41477-017-0063-z.

(33) Pasupathy, K.; Lin, S.; Hu, Q.; Luo, H.; Ke, P. C. Direct Plant Gene Delivery with a Poly(Amidoamine) Dendrimer. *Biotechnology Journal* **2008**, *3* (8), 1078–1082. https://doi.org/10.1002/biot.200800021.

(34) Jiang, L.; Ding, L.; He, B.; Shen, J.; Xu, Z.; Yin, M.; Zhang, X. Systemic Gene Silencing in Plants Triggered by Fluorescent Nanoparticle-Delivered Double-Stranded RNA. *Nanoscale* **2014**, *6* (17), 9965–9969. https://doi.org/10.1039/C4NR03481C.

(35) Naqvi, S.; Maitra, A. N.; Abdin, M. Z.; Akmal, M.; Arora, I.; Samim, M. Calcium Phosphate Nanoparticle Mediated Genetic Transformation in Plants. *J. Mater. Chem.* **2012**, *22* (8), 3500–3507. https://doi.org/10.1039/C2JM11739H.

(36) Mitter, N.; Worrall, E. A.; Robinson, K. E.; Li, P.; Jain, R. G.; Taochy, C.; Fletcher, S. J.; Carroll, B. J.; Lu, G. Q. (Max); Xu, Z. P. Clay Nanosheets for Topical Delivery of RNAi for Sustained Protection against Plant Viruses. *Nature Plants* **2017**, *3* (2), 1–10. https://doi.org/10.1038/nplants.2016.207.

(37) Demirer, G. S.; Zhang, H.; Matos, J. L.; Goh, N. S.; Cunningham, F. J.; Sung, Y.; Chang, R.; Aditham, A. J.; Chio, L.; Cho, M.-J.; Staskawicz, B.; Landry, M. P. High Aspect Ratio Nanomaterials Enable Delivery of Functional Genetic Material without DNA Integration in Mature Plants. *Nat. Nanotechnol.* **2019**, *14* (5), 456–464. https://doi.org/10.1038/s41565-019-0382-5.

(38) Brinkman, E. K.; Chen, T.; Amendola, M.; van Steensel, B. Easy Quantitative Assessment of Genome Editing by Sequence Trace Decomposition. *Nucleic Acids Res* **2014**, *42* (22), e168. https://doi.org/10.1093/nar/gku936.

(39) Gonzalez Grandio, E.; Demirer, G.; Jackson, C.; Yang, D.; Ebert, S.; Molawi, K.; Keller, H.; Landry, M. Carbon Nanotube Biocompatibility in Plants Is Determined by Their Surface Chemistry. *Journal of Nanobiotechnology* **2021**, *19*. https://doi.org/10.1186/s12951-021-01178-8.

(40) Ali, Z.; Serag, M. F.; Demirer, G. S.; Torre, B.; di Fabrizio, E.; Landry, M. P.; Habuchi, S.; Mahfouz, M. DNA–Carbon Nanotube Binding Mode Determines the Efficiency of Carbon Nanotube-Mediated DNA Delivery to Intact Plants. *ACS Appl. Nano Mater.* **2022**, *5* (4), 4663–4676. https://doi.org/10.1021/acsanm.1c03482.

(41) Demirer, G. S.; Zhang, H.; Goh, N. S.; González-Grandío, E.; Landry, M. P. Carbon Nanotube–Mediated DNA Delivery without Transgene Integration in Intact Plants. *Nat Protoc* **2019**, *14* (10), 2954–2971. https://doi.org/10.1038/s41596-019-0208-9.

(42) Naeem, M.; Majeed, S.; Hoque, M. Z.; Ahmad, I. Latest Developed Strategies to Minimize the Off-Target Effects in CRISPR-Cas-Mediated Genome Editing. *Cells* **2020**, *9* (7), 1608. https://doi.org/10.3390/cells9071608.

(43) Shibata, M.; Nishimasu, H.; Kodera, N.; Hirano, S.; Ando, T.; Uchihashi, T.; Nureki, O. Real-Space and Real-Time Dynamics of CRISPR-Cas9 Visualized by High-Speed Atomic Force Microscopy. *Nat Commun* **2017**, *8* (1), 1430. https://doi.org/10.1038/s41467-017-01466-8.

(44) Jinek, M.; Jiang, F.; Taylor, D. W.; Sternberg, S. H.; Kaya, E.; Ma, E.; Anders, C.; Hauer, M.; Zhou, K.; Lin, S.; Kaplan, M.; Iavarone, A. T.; Charpentier, E.; Nogales, E.; Doudna, J. A. Structures of Cas9 Endonucleases Reveal RNA-Mediated Conformational Activation. *Science* **2014**, *343* (6176), 1247997. https://doi.org/10.1126/science.1247997.

(45) Chen, K.; Jiang, S.; Hong, Y.; Li, Z.; Wu, Y.-L.; Wu, C. Cationic Polymeric Nanoformulation: Recent Advances in Material Design for CRISPR/Cas9 Gene Therapy. *Progress in Natural Science: Materials International* **2019**, *29* (6), 617–627. https://doi.org/10.1016/j.pnsc.2019.10.003.

(46) Nguyen, D.; Roth, T.; Li, P.; Chen, P.; Apathy, R.; Mamedov, M.; Vo, L.; Tobin, V.; Goodman, D.; Shifrut, E.; Bluestone, J.; Puck, J.; Szoka, F.; Marson, A. Polymer-Stabilized Cas9 Nanoparticles and Modified Repair Templates Increase Genome Editing Efficiency. *Nature Biotechnology* **2020**, *38*, 1–6. https://doi.org/10.1038/s41587-019-0325-6.

(47) Pinals, R. L.; Yang, D.; Rosenberg, D. J.; Chaudhary, T.; Crothers, A. R.; Iavarone, A. T.; Hammel, M.; Landry, M. P. Quantitative Protein Corona Composition and Dynamics on Carbon Nanotubes in Biological Environments. *Angewandte Chemie International Edition* **2020**, *59* (52), 23668–23677. https://doi.org/10.1002/anie.202008175.

(48) Le Trong, I.; Wang, Z.; Hyre, D. E.; Lybrand, T. P.; Stayton, P. S.; Stenkamp, R. E. Streptavidin and Its Biotin Complex at Atomic Resolution. *Acta Cryst D* **2011**, *67* (9), 813–821. https://doi.org/10.1107/S0907444911027806.

(49) Green, N. M. Avidin. In *Advances in Protein Chemistry*; Anfinsen, C. B., Edsall, J. T., Richards, F. M., Eds.; Academic Press, 1975; Vol. 29, pp 85–133. https://doi.org/10.1016/S0065-3233(08)60411-8.

(50) Chio, L.; Pinals, R. L.; Murali, A.; Goh, N. S.; Landry, M. P. Covalent Surface Modification Effects on Single-Walled Carbon Nanotubes for Targeted Sensing and Optical Imaging. *Advanced Functional Materials* **2020**, *30* (17), 1910556. https://doi.org/10.1002/adfm.201910556.

(51) *Engineering Soluble Monomeric Streptavidin with Reversible Biotin Binding Capability* - Journal of Biological Chemistry*. https://www.jbc.org/article/S0021-9258(20)61497-1/fulltext (accessed 2022-07-17).

(52) Wang, S.; Humphreys, E. S.; Chung, S.-Y.; Delduco, D. F.; Lustig, S. R.; Wang, H.; Parker, K. N.; Rizzo, N. W.; Subramoney, S.; Chiang, Y.-M.; Jagota, A. Peptides with Selective Affinity for Carbon Nanotubes. *Nature Mater* **2003**, *2* (3), 196–200. https://doi.org/10.1038/nmat833.

(53) Zuckermann, R. N. Peptoid Origins. *Peptide Science* **2011**, *96* (5), 545–555. https://doi.org/10.1002/bip.21573.

(54) *Comparison of the proteolytic susceptibilities of homologous L-amino acid, D-amino acid, and N-substituted glycine peptide and peptoid oligomers - Miller - 1995 - Drug Development Research - Wiley Online Library*. https://onlinelibrary.wiley.com/doi/abs/10.1002/ddr.430350105 (accessed 2022-07-17).

(55) Kim, J. H.; Kim, S. C.; Kline, M. A.; Grzincic, E. M.; Tresca, B. W.; Cardiel, J.; Karbaschi, M.; Dehigaspitiya, D. C.; Chen, Y.; Udumula, V.; Jian, T.; Murray, D. J.; Yun, L.; Connolly, M. D.; Liu, J.; Ren, G.; Chen, C.-L.; Kirshenbaum, K.; Abate, A. R.; Zuckermann, R. N. Discovery of Stable and Selective Antibody Mimetics from Combinatorial Libraries of Polyvalent, Loop-

Functionalized Peptoid Nanosheets. *ACS Nano* **2020**, *14* (1), 185–195. https://doi.org/10.1021/acsnano.9b07498.

(56) Chio, L.; Del Bonis-O'Donnell, J. T.; Kline, M. A.; Kim, J. H.; McFarlane, I. R.; Zuckermann, R. N.; Landry, M. P. Electrostatic Assemblies of Single-Walled Carbon Nanotubes and Sequence-Tunable Peptoid Polymers Detect a Lectin Protein and Its Target Sugars. *Nano Lett.* **2019**. https://doi.org/10.1021/acs.nanolett.8b04955.

(57) Zuckermann, R. N.; Kerr, J. M.; Kent, S. B. H.; Moos, W. H. Efficient Method for the Preparation of Peptoids [Oligo(N-Substituted Glycines)] by Submonomer Solid-Phase Synthesis. *J. Am. Chem. Soc.* **1992**, *114* (26), 10646–10647. https://doi.org/10.1021/ja00052a076.

(58) Hendel, A.; Bak, R. O.; Clark, J. T.; Kennedy, A. B.; Ryan, D. E.; Roy, S.; Steinfeld, I.; Lunstad, B. D.; Kaiser, R. J.; Wilkens, A. B.; Bacchetta, R.; Tsalenko, A.; Dellinger, D.; Bruhn, L.; Porteus, M. H. Chemically Modified Guide RNAs Enhance CRISPR-Cas Genome Editing in Human Primary Cells. *Nat Biotechnol* **2015**, *33* (9), 985–989. https://doi.org/10.1038/nbt.3290.

(59) Shlyakhtenko, L. S.; Gall, A. A.; Lyubchenko, Y. L. Mica Functionalization for Imaging of DNA and Protein-DNA Complexes with Atomic Force Microscopy. *Methods Mol Biol* **2013**, *931*, 10.1007/978-1-62703-056-4_14. https://doi.org/10.1007/978-1-62703-056-4_14.

(60) Demirer, G. S.; Zhang, H.; Goh, N. S.; Pinals, R. L.; Chang, R.; Landry, M. P. Carbon Nanocarriers Deliver SiRNA to Intact Plant Cells for Efficient Gene Knockdown. *Science Advances* **2020**, *6* (26), eaaz0495. https://doi.org/10.1126/sciadv.aaz0495.

(61) *Efficient Transient Gene Knock-down in Tobacco Plants Using Carbon Nanocarriers — BIO-PROTOCOL*. https://bio-protocol.org/e3897 (accessed 2022-07-19).

(62) Martin-Ortigosa, S.; Valenstein, J. S.; Lin, V. S.-Y.; Trewyn, B. G.; Wang, K. Gold Functionalized Mesoporous Silica Nanoparticle Mediated Protein and DNA Codelivery to Plant Cells Via the Biolistic Method. *Advanced Functional Materials* **2012**, *22* (17), 3576–3582. https://doi.org/10.1002/adfm.201200359.

(63) Martin-Ortigosa, S.; Peterson, D. J.; Valenstein, J. S.; Lin, V. S.-Y.; Trewyn, B. G.; Lyznik, L. A.; Wang, K. Mesoporous Silica Nanoparticle-Mediated Intracellular Cre Protein Delivery for Maize Genome Editing via LoxP Site Excision,. *Plant Physiology* **2014**, *164* (2), 537–547. https://doi.org/10.1104/pp.113.233650.

(64) Liu, J.; Wang, F. H.; Wang, L. L.; Xiao, S. Y.; Tong, C. Y.; Tang, D. Y.; Liu, X. M. Preparation of Fluorescence Starch-Nanoparticle and Its Application as Plant Transgenic Vehicle. *Journal of Central South University of Technology (English Edition)* **2008**, *15* (6), 768–773. https://doi.org/10.1007/s11771-008-0142-4.

(65) Hao, Y.; Yang, X.; Shi, Y.; Song, S.; Xing, J.; Marowitch, J.; Chen, J. J. Magnetic Gold Nanoparticles as a Vehicle for Fluorescein Isothiocyanate and DNA Delivery into Plant Cells. *Botany* **2013**, *91* (7), 457–466. https://doi.org/10.1139/cjb-2012-0281.

(66) Finiuk, N.; Buziashvili, A.; Burlaka, O.; Zaichenko, A.; Mitina, N.; Miagkota, O.; Lobachevska, O.; Stoika, R.; Blume, Y.; Yemets, A. Investigation of Novel Oligoelectrolyte Polymer Carriers for Their Capacity of DNA Delivery into Plant Cells. *Plant Cell, Tissue and Organ Culture* **2017**, *131* (1), 27–39. https://doi.org/10.1007/s11240-017-1259-7.

(67) Zhao, X.; Meng, Z.; Wang, Y.; Chen, W.; Sun, C.; Cui, B.; Cui, J.; Yu, M.; Zeng, Z.; Guo, S.; Luo, D.; Cheng, J. Q.; Zhang, R.; Cui, H. Pollen Magnetofection for Genetic Modification with Magnetic Nanoparticles as Gene Carriers. *Nature Plants* **2017**, *3* (12), 956–964. https://doi.org/10.1038/s41477-017-0063-z.

(68) Naqvi, S.; Maitra, A. N.; Abdin, M. Z.; Akmal, Md.; Arora, I.; Samim, Md. Calcium Phosphate Nanoparticle Mediated Genetic Transformation in Plants. *Journal of Materials Chemistry* **2012**, *22* (8), 3500. https://doi.org/10.1039/c2jm11739h.

(69) Pasupathy, K.; Lin, S.; Hu, Q.; Luo, H.; Ke, P. C. Direct Plant Gene Delivery with a Poly(Amidoamine) Dendrimer. *Biotechnology Journal* **2008**, *3* (8), 1078–1082. https://doi.org/10.1002/biot.200800021.

(70) Jiang, L.; Ding, L.; He, B.; Shen, J.; Xu, Z.; Yin, M.; Zhang, X. Systemic Gene Silencing in Plants Triggered by Fluorescent Nanoparticle-Delivered Double-Stranded RNA. *Nanoscale* **2014**, *6* (17), 9965. https://doi.org/10.1039/C4NR03481C.

(71) Chang, F.-P.; Kuang, L.-Y.; Huang, C.-A.; Jane, W.-N.; Hung, Y.; Hsing, Y. C.; Mou, C.-Y. A Simple Plant Gene Delivery System Using Mesoporous Silica Nanoparticles as Carriers. *Journal of Materials Chemistry B* **2013**, *1* (39), 5279. https://doi.org/10.1039/c3tb20529k.